Optical and Structural Characterization of Semiconductors for Mid-Wave Infrared Applications

MASTER'S DEFENSE

Haley B. Woolf

College of Arts and Sciences

Department of Physics



BE BOLD. Shape the Future. New Mexico State University

Acknowledgements

COMMITTEE:

- Dr. Stefan Zollner
- Dr. Rigo Carrasco
- Dr. Michael Paolone
- Dr. Miranda van Iersel

COLLABORATORS:

- Dr. Matt Kim, QuantTera
- Dr. Preston Webster et al., Air Force Research Lab
- Dr. Jose Menendez, Arizona State University
- Dr. John Kouvetakis, Arizona State University
- Matthew Mircovich, Arizona State University

FUNDING:

- Air Force Research Laboratory (FA9453-23-2-0001)
 - Air Force Office of Scientific Research (FA9550-24-1-0061)
 - National Science Foundation (DMR-2235447, DMR-2423992)
 - Scalable Asymmetric Lifecycle Engagement (W5P1J-22-9-3009)











RESEARCH PEERS:

- Jaden Love
- Carlos Armeta
- Danissa Ortega
- Sonam Yadav
- Yoshitha Hettige
- Carola Emminger
- Aaron Lopez Gonzalez
- Gabriel Ruiz



Vita:

2022: **Engineering Intern**

SVAD, WSMR

Secret Clearance Activated

2023: **Optoelectronics Intern** *MESA, SNL*

2024: **B.S. Engineering Physics** *NMSU*

2024: AFRL Scholar

RVSU, AFRL

2021-2025: **Research Assistant** *NMSU*

Posters:

- H. B. Woolf, M. Kim, C. Emminger, C. Armenta, S. Zollner. Optical and X-Ray Characterization of Ge₁₋
 _vSn_v alloy on GaAs. Presented at:
 - American Physical Society March Meeting, 14-18 March 2022, Chicago, IL.
- D. Ortega, H. B. Woolf, A. Moses, C. Armenta, J. Love, S. Yadav, M. Mircovich, J. Kouvetakis, J. Menendez, S. Zollner. Optical and Structural Properties of Group-IV Oxides Produced by Rapid Thermal Oxidation. Presented at:
 - 50th Conference on the Physics and Chemistry of Surfaces and Interfaces, 19-23 January 2025, Kailua-Kona, HI
 - 10th International Conference on Spectroscopic Ellipsometry, 8-13 June 2025, Boulder CO.
- H. B. Woolf, R. Carrasco, P. Webster, A. Newell, A. Duchane, C. Morath, D. Maestas. Temperature-Dependent Recombination Rate Analysis of the Minority Carrier Lifetime in Mid-Wave Infrared Antimonide-based Materials. Presented at:
 - 50th Conference on the Physics and Chemistry of Surfaces and Interfaces, 19-23 January 2025, Kailua-Kona, HI.

Presentation:

- H. B. Woolf, M. Kim, C. Emminger, C. Armenta, S. Zollner. Optical and X-Ray Characterization of Ge₁₋
 _vSn_v alloy on GaAs. Presented at:
 - Undergraduate Research and Creative Arts Symposium, 29 April 2022, Las Cruces, NM
 - American Vacuum Society 67th International Symposium, 6-11 November 2022, Pittsburgh, PA.

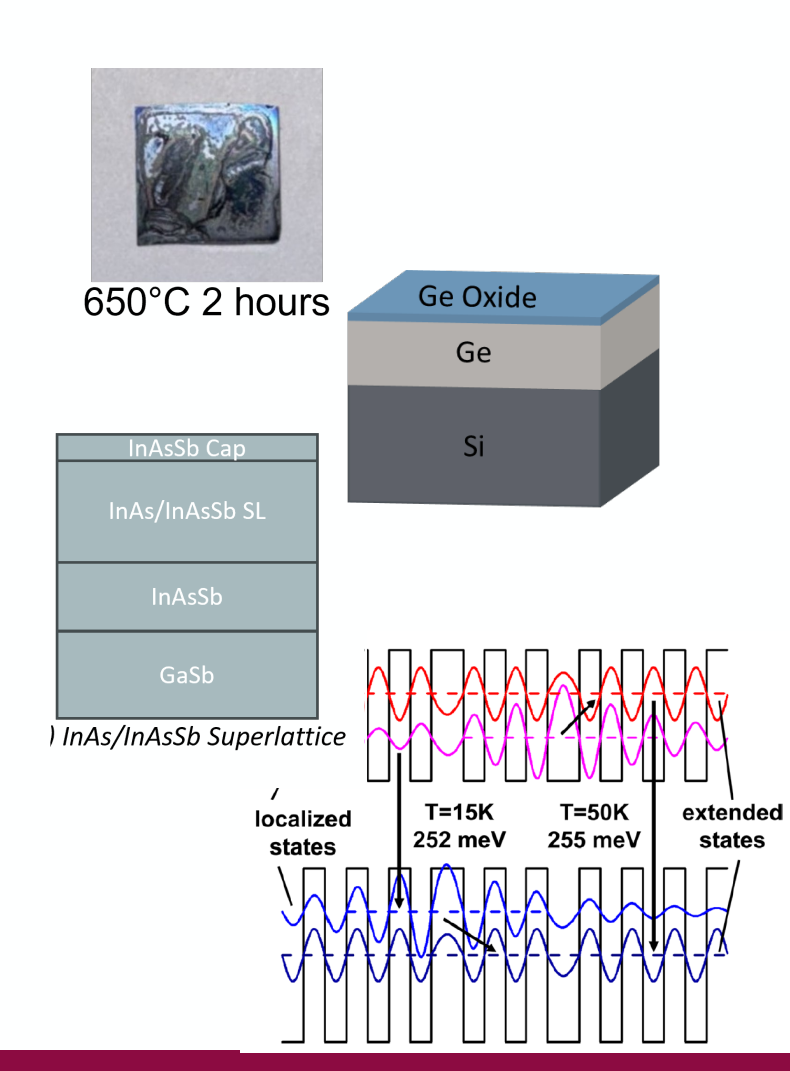
Awards

- Ken Hass Outstanding Poster Award Forum on Industrial and Applied Physics (FIAP) Awarded at:
 - American Physical Society March Meeting, 14-18 March 2022, Chicago, IL.



Outline

- Optical and Structural Properties of Group-IV Oxides Produced by Rapid Thermal Annealing
 - Experimental Methods
 - Rapid Thermal Oxidation
 - Ge on Si Results
 - GeSn on Si Results
- Temperature-Dependent Recombination Rate Analysis of Minority Carrier Lifetime in Mid-Wave Infrared Antimonide-Based Devices
 - Recombination
 - Previous Observations-Strain Engineering & Localization Effects
 - Methodology
 - Results



Motivation

- Engineering semiconductors to have tunable infrared absorption
 - Short-Wave (0.9-2.5 μm), Mid-Wave (3-5 μm), Long-Wave (8-14 μm)
- Ge-based and GeSn-based devices are commonly used in Complimentary Metal-Oxide-Semiconductor (CMOS) devices.
- Passivation is utilized in device fabrication making it important to understand the surface's thermal stability.
- Mid-Wave are often made with III-V materials, like In(Ga)As/InAsSb superlattices.
- Used in telecommunications, thermal imaging, and missile tracking.



Optical and Structural Properties of Group-IV Oxides Produced by Rapid Thermal Annealing



Reciprocal Space & Bragg's Law

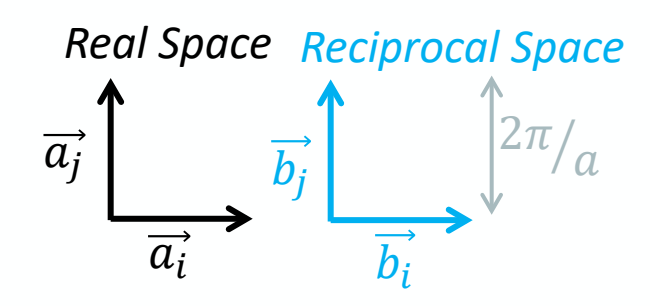
- Crystal = Lattice + Basis
 - Lattice points with identical orientation throughout an array
 - Basis identical groups of atoms attached to a lattice
- Each point defined by a **Position Vector** in real space

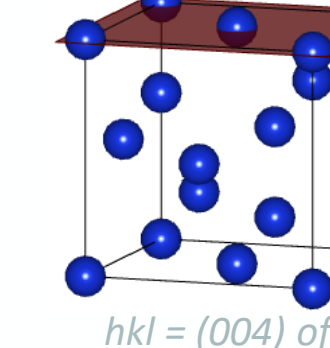
$$(\overrightarrow{r'} = u_1 \overrightarrow{a_1} + u_2 \overrightarrow{a_2} + u_3 \overrightarrow{a_3})$$

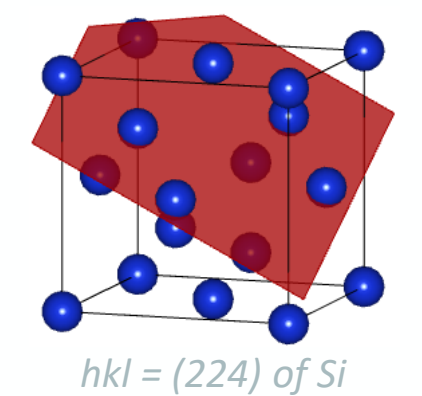
• Lattice planes are described by the orientation and spacing of the atomic layers, defined by **Reciprocal Space Vectors**

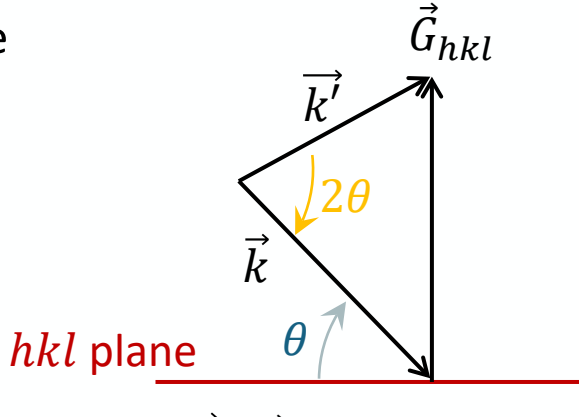
$$(\vec{G} = v_1 \overrightarrow{b_1} + v_2 \overrightarrow{b_2} + v_3 \overrightarrow{b_3}; G = \frac{2\pi}{d_{hkl}})$$

- X-ray reflections of the crystals are determined by \vec{G} and the Elastic Scattering Theory where $\Delta \vec{k} = \vec{k'} \vec{k} = \vec{G}$; $\left| \vec{k} \right| = \frac{2\pi}{\lambda}$
- These relationships lead to **Bragg's Law**: $2d_{hkl}\sin(\theta) = \lambda$









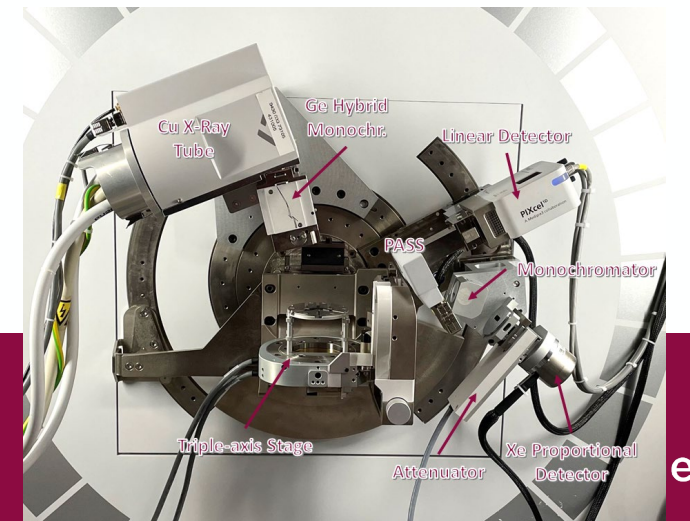
 $\vec{k} \cdot \vec{G} = kG \sin(\theta)$

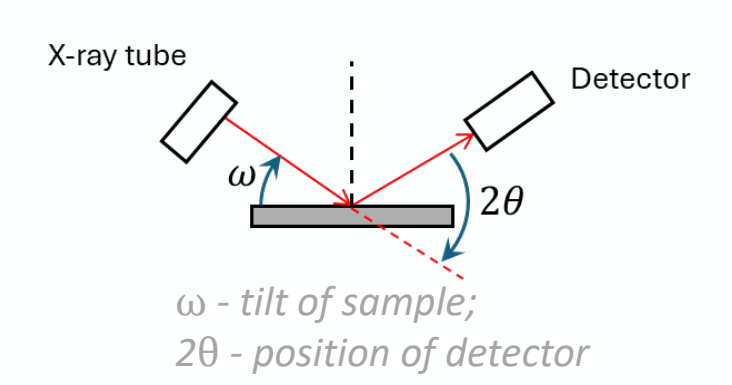


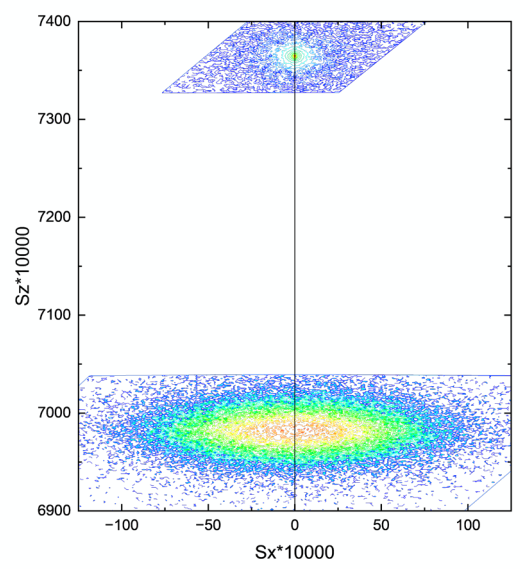
X-Ray Diffraction (XRD)

- Powder XRD: crystal quality, low resolution
 - Beam conditioner (Bragg-Brentano) reduces divergence of x-rays with slits
 - $2\theta \omega$ move together over a large range
- High Resolution XRD: strain, lattice constants, composition
 - Beam conditioner (Hybrid Monochromator) creates collimated beam with one wavelength
 - ω rocking curves, $\omega 2\theta$ (short range), reciprocal space maps (RSM)

PANalytical Empyrean X-Ray Diffractometer



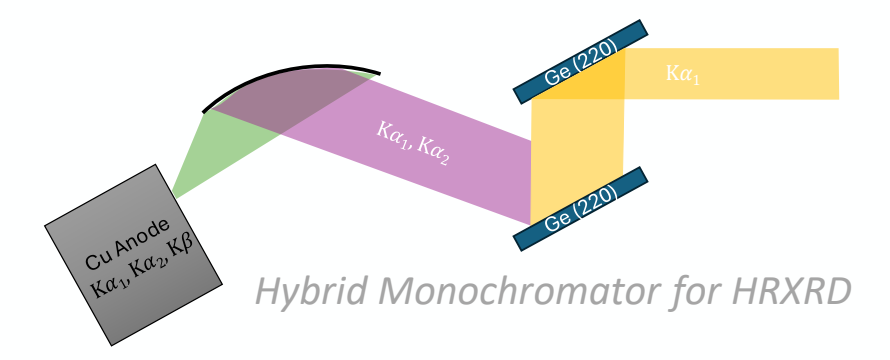




(004) RSM of GeSn on Si

$$s_x = \frac{q_x}{2\pi} = \frac{1}{\lambda} [\cos(\omega) - \cos(2\theta - \omega)]$$

$$s_z = \frac{q_z}{2\pi} = \frac{1}{\lambda} [\sin(\omega) + \sin(2\theta - \omega)]$$



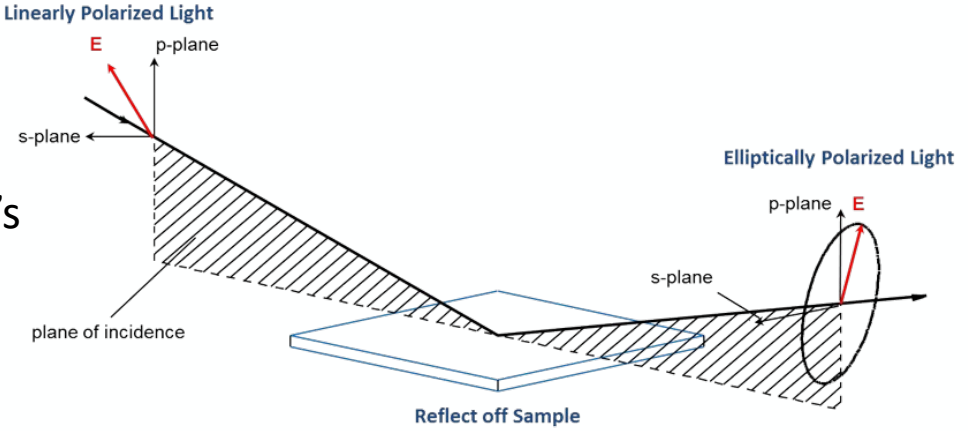
P. F. Fewster, *X-Ray Scattering From Semiconductors and Other Materials,* (World Scientific Pub. Co. 2015).

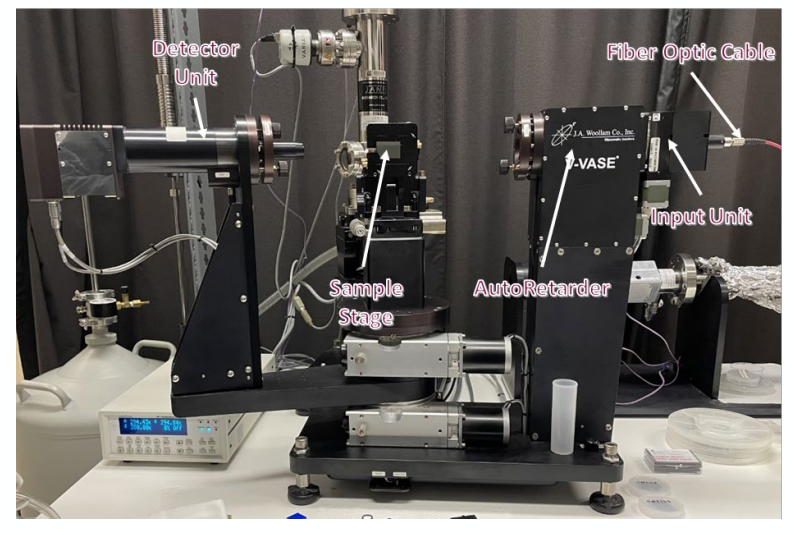
Ellipsometry

- Study of the change in polarization as light interacts with a material's structure.
- Ellipsometry Equation: $\rho = \tan \Psi \exp(i\Delta) = \frac{r_p}{r_s}$
 - Amplitude Ratio: $tan(\Psi) = \left| \frac{r_p}{r_s} \right|$
 - Phase Difference: $\Delta = \delta_p \delta_s$
- Reflection Coefficients:

•
$$r_p = \frac{E_p^{reflec}}{E_p^{inc}} = \frac{\widetilde{N_1}\cos\theta_0 - \widetilde{N_0}\cos\theta_1}{\widetilde{N_1}\cos\theta_0 + \widetilde{N_0}\cos\theta_1},$$
 $r_S = \frac{E_S^{reflec}}{E_S^{inc}} = \frac{\widetilde{N_0}\cos\theta_0 - \widetilde{N_1}\cos\theta_1}{\widetilde{N_0}\cos\theta_0 + \widetilde{N_1}\cos\theta_1}$

- Complex Index of Refraction: $\widetilde{N} = n + ik$
 - Index of Refraction: n = c/v
 - Extinction Coefficient: $k = \alpha \frac{\lambda}{4\pi}$
- Complex Dielectric Function: $\tilde{\varepsilon} = \varepsilon_1 + i\varepsilon_2 = \widetilde{N}^2$
- Multiple reflections and interferences modify the refraction coefficients where the film phase thickness quantifies the phase difference between the layers:
 - $\beta = \frac{2\pi d}{\lambda} \widetilde{N_1} \cos \theta_1$





J.A. Woollam UV-VASE Ellipsometer



H. Fujiwara, Spectroscopic Ellipsometry (John Wiley & Sons, 2007).

J. A. Woollam Co., Guide to Using WVASE32 (2017).

Introduction

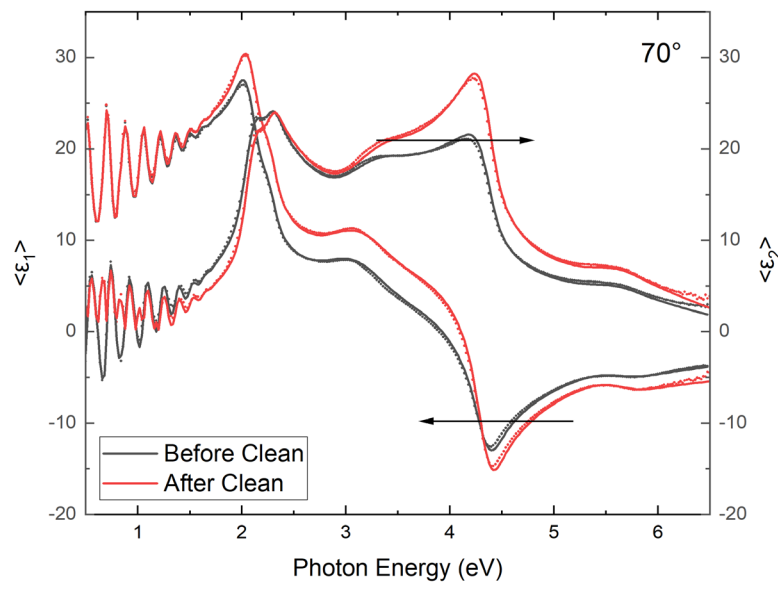
- Ge(Sn) on Si samples, %Sn = 6.9%, grown by the group of Kouvetakis at ASU by chemical vapor deposition
- GeO₂ is identified as a promising piezoelectric material, converts mechanical stress to electrical energy.
- Ge has an indirect bandgap that transitions towards a direct bandgap with Sn incorporation.
- Performance of these devices depend on the quality of the GeSn layer.



Rapid Thermal Oxidation Procedure

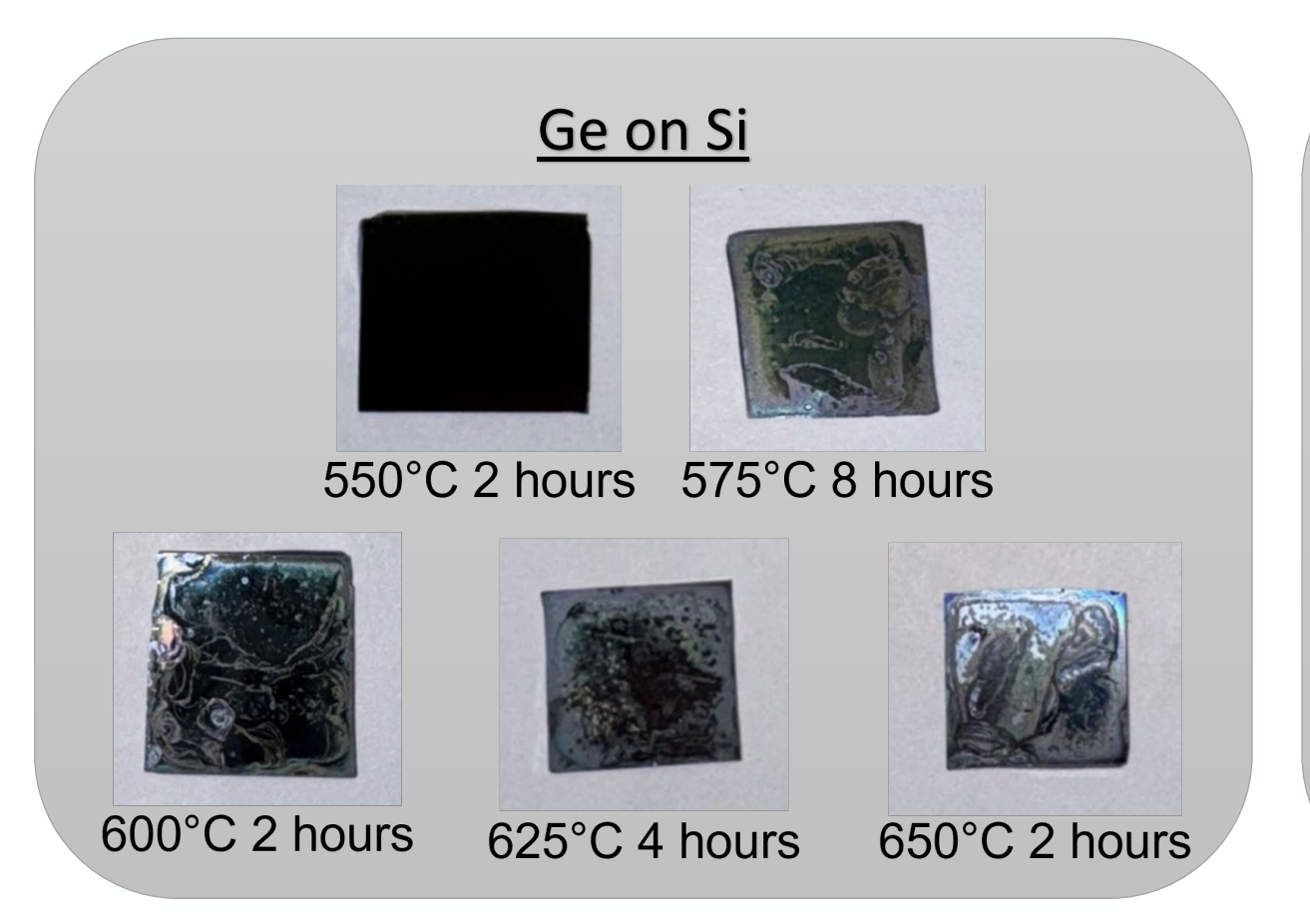
- Ultrasonically cleaned in deionized water for 15 mins, then dried with nitrogen gas
- MILA-5000 Mini Lamp Annealer (ULVAC-RIKO, Inc.)
 - Oxygen Flow Rate: 0.2 L/min Pressure: 2.7 atm
- Heats up:1 min, at temp:specific time, cools to room temp:20-30 mins
 - Ge on Si: 550°C-650°C for 2,4,8 hours
- Ellipsometry was used to measure the thicknesses
 - Before Clean, Before Anneal;
 - After Clean, Before Anneal;
 - After Clean, After Anneal

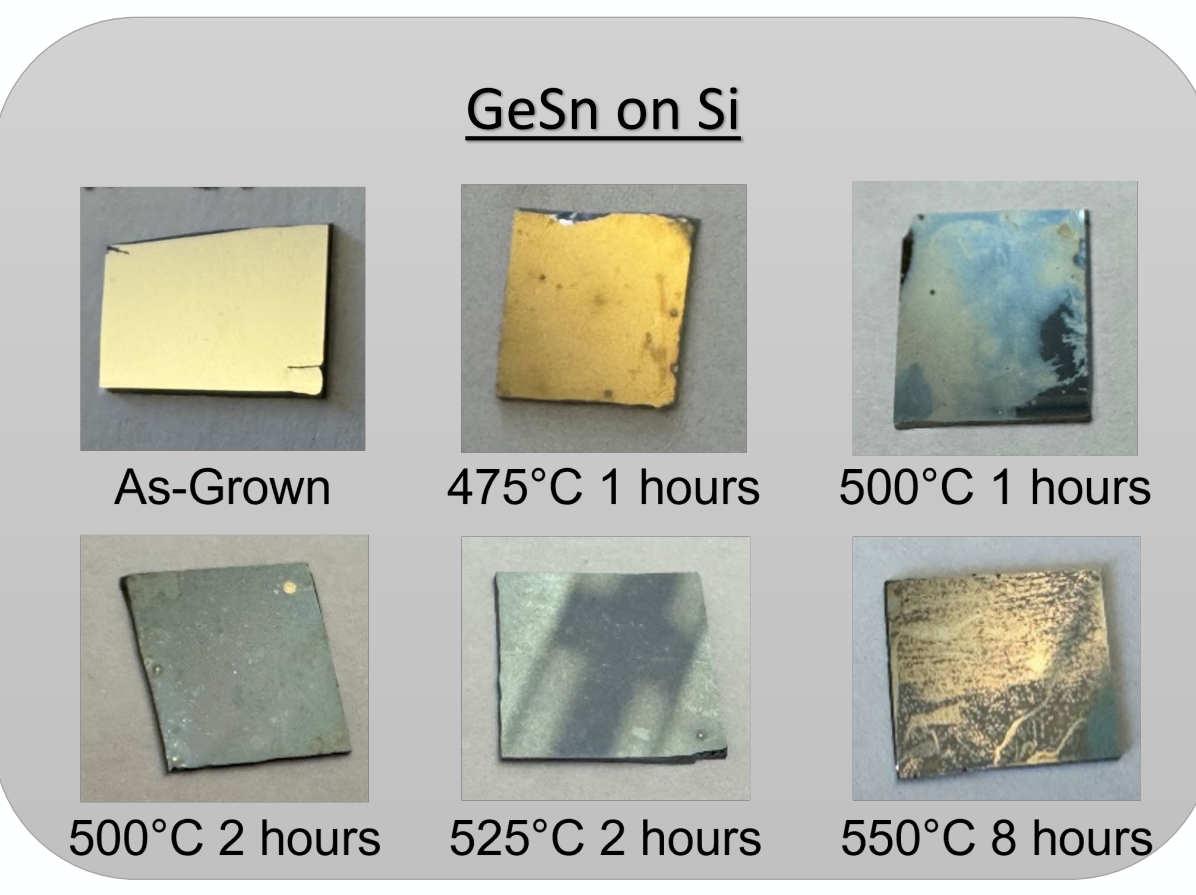
	Avg. As-Received Avg. After Clean Oxide Thickness (Å) Oxide Thickness (Å	
Ge on Si	26	11
GeSn on Si	38	25



Pseudodielectric function for Ge on Si before and after cleaning.

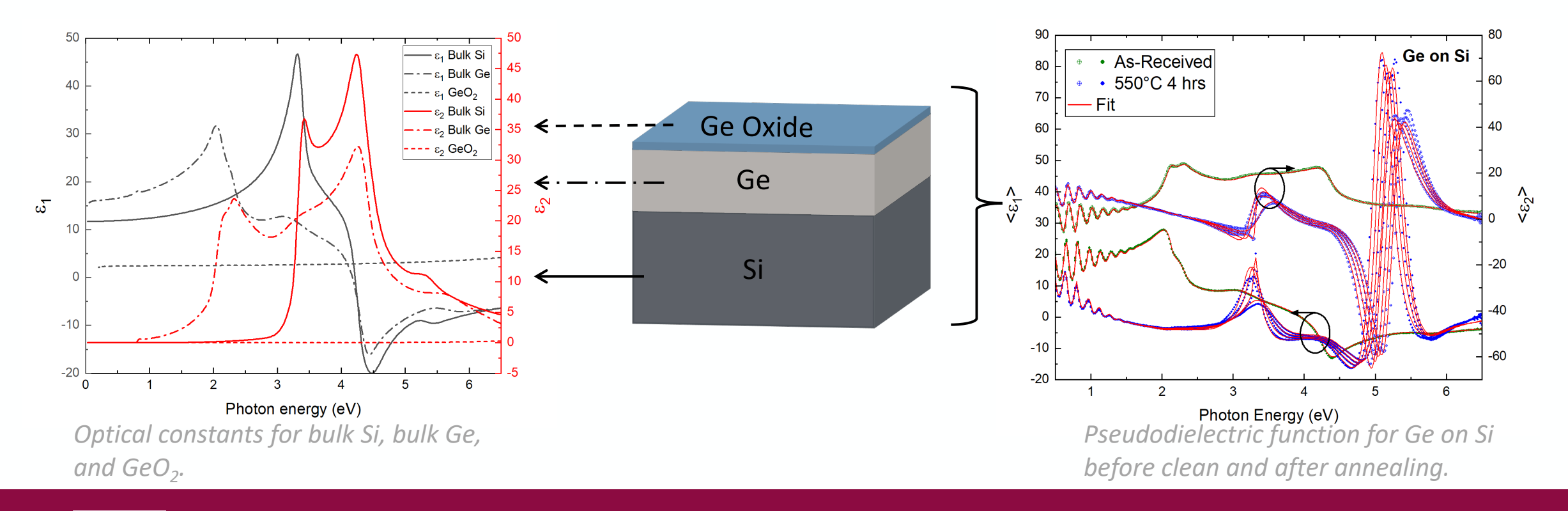
Surface Decolorization





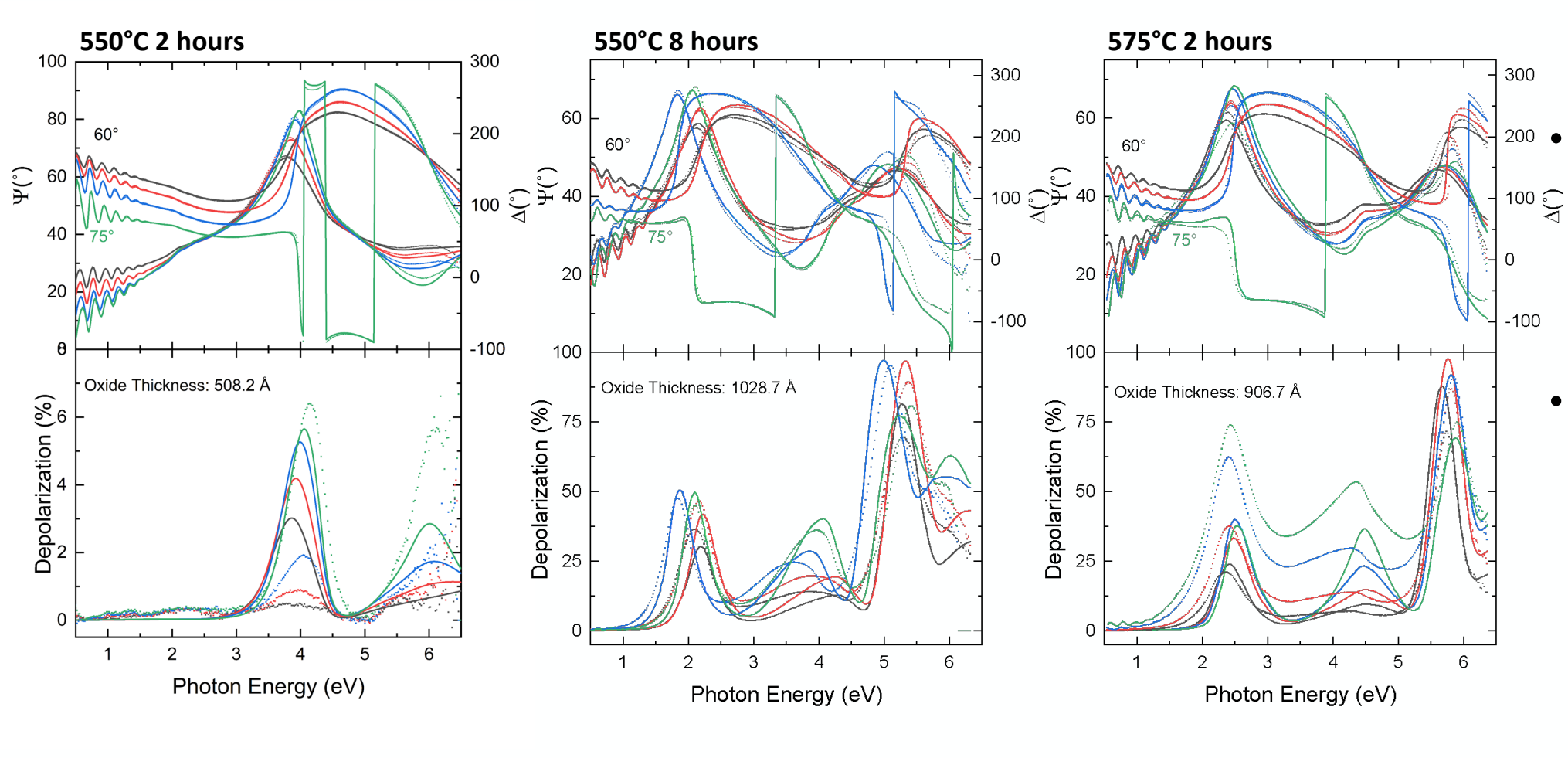
Ge on Si: Ellipsometry Model - UV

- Optical constants for each layer are used to model the data to determine the thicknesses.
- Modeling included non-uniformity in the Ge oxide layer





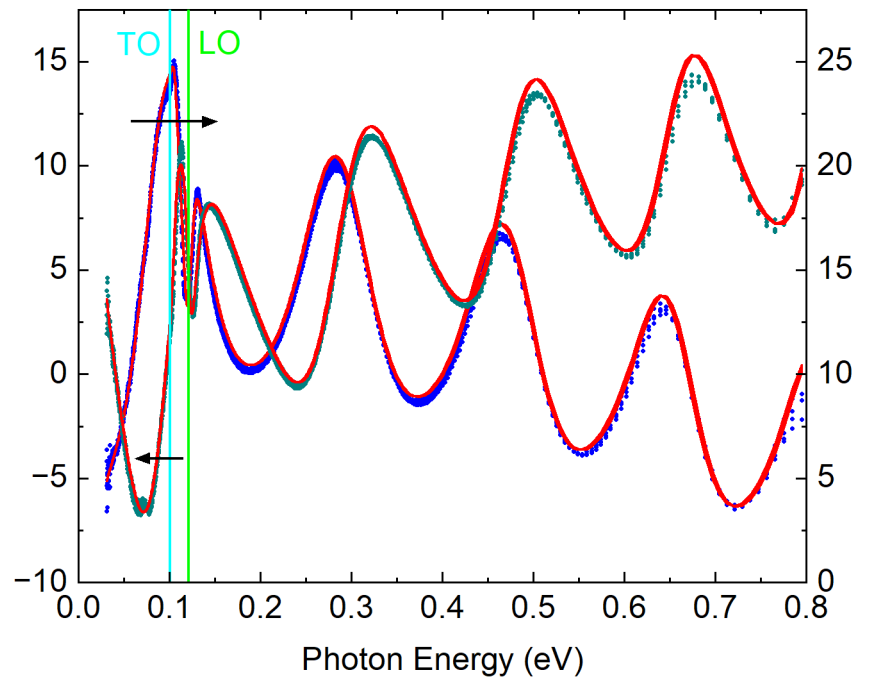
Ge on Si: Depolarization



- Ellipsometric angles (Ψ, Δ) and depolarization for three different growths modeled with non-uniformity in the GeO_2 .
- Depolarization increases with layer thickness as seen by the 550°C with increased time.

Ge on Si: Phonon Modes in IR

- Samples were measured with IRVASE from 0.03-0.8 eV
- Model: Dude superposition in the Bulk Si and Bulk Ge layers; Oxide with a general oscillator layer
- Anneal at 550°C for 4 hrs,
 - Transverse Optical (TO) Phonon Frequency = 0.10 eV
 - Longitudinal Optical (LO) Phonon Frequencies = 0.12 eV
- Armand et al. measured anisotropic trigonal GeO₂ modes from 0.105-0.124 eV



Pseudodielectric of Ge on Si annealed at 550°C for 4 hours with labeled TO and LO phonon frequencies.

TO: Peak of ε_2

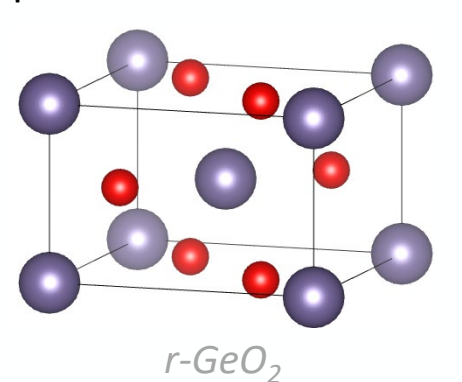
LO: Peak of Loss Function, $\operatorname{Im}\left(-\frac{1}{\varepsilon}\right) = \frac{\varepsilon_2}{\varepsilon_1^2 + \varepsilon_2^2}$

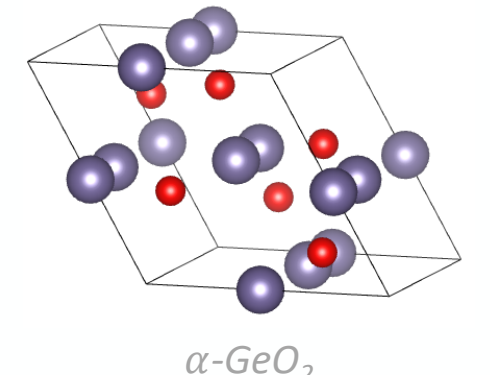


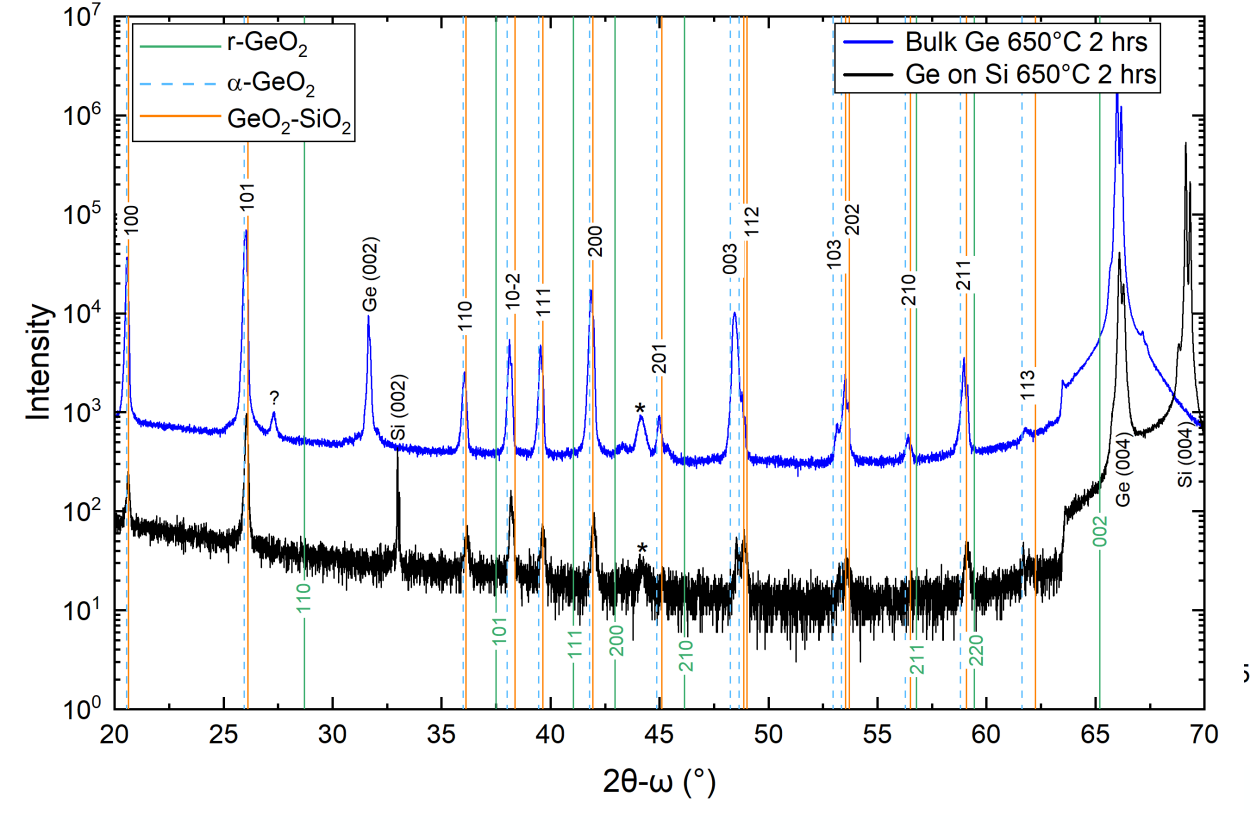
J. A. Woollam Co., Guide to Using WVASE32 (2017).

Ge on Si: After Anneal Powder XRD

- In powder spectra, (004) peaks for bulk Ge and Si are consistent for Si (100) orientation
- Peaks for (002) are forbidden but are visible due to multiple diffraction – one or more diffraction condition is satisfied
- Other peaks are compared to possible phases of GeO₂:
 - Rutile GeO₂ tetragonal, more thermodynamically stable
 - α GeO₂ trigonal, metastable
 - <u>SiO₂-substituted GeO₂</u> distorts crystal's structural parameters









Ge on Si: Cross-Sectional EDX

• (1) Si Substrate

Si (Wt%)	Ge	0	С	Other
96.8(0.4)	0	0.5(0.1)	2.7(10.4)	0

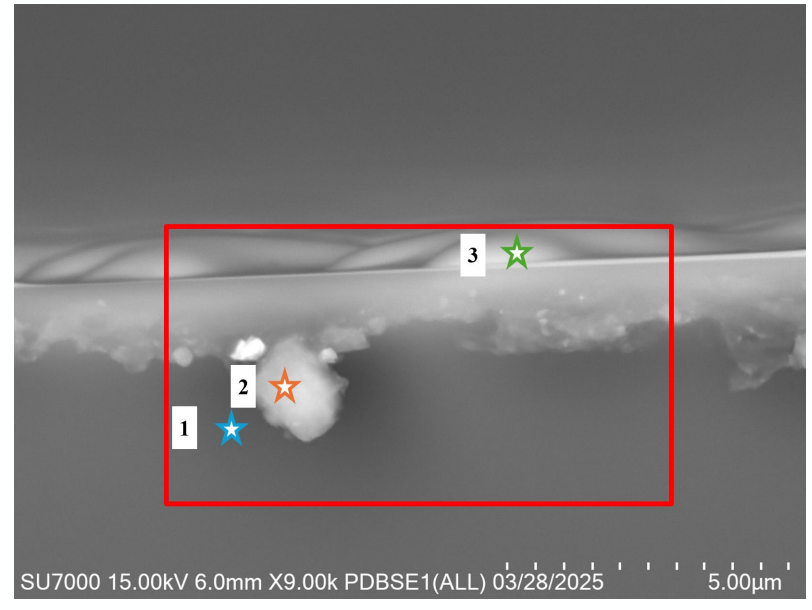
• (2) Unknown; Artifact from Cleave

Si (Wt%)	Ge	0	С	Other
47.1(0.3)	0	25.4(0.2)	20.1(0.5)	7.45(0.3)

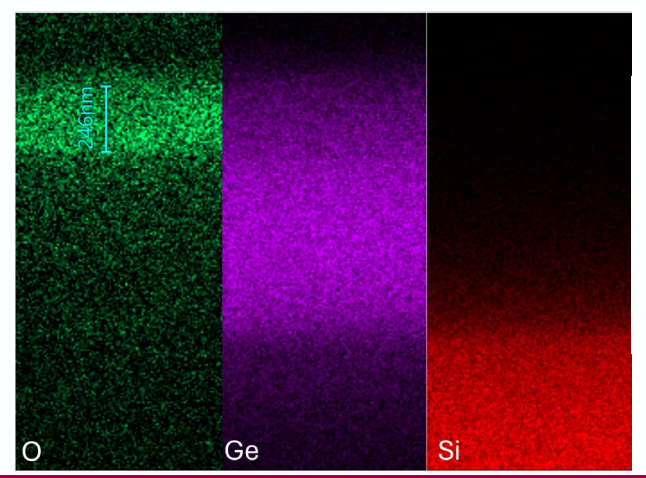
• (3) Sample's Surface

Si (Wt%)	Ge	0	С	Other
20.0(0.1)	41.0(0.2)	29.4(0.2)	9.62(0.3)	0

- Although, EDX may suggest Si is present in the oxide, the possibility is **uncertain due to Si needing to migrate** through the entire Ge layer.
- FROM POWDER: Other possibility is that the oxide may be composed of only Ge showing a reduced lattice constant that increases density during annealing



Cross-sectional SEM image of Ge on Si after 650°C for 2 hours.



EDX measurements of Ge on Si after 575°C for 8 hours. Oxide measured by EDX and ellipsometry were 2460 Å and 2409 Å.

Ge on Si: High Resolution XRD

$$s_x = \frac{q_x}{2\pi} = \frac{1}{\lambda} [\cos(\omega) - \cos(2\theta - \omega)]$$

$$s_z = \frac{q_z}{2\pi} = \frac{1}{\lambda} [\sin(\omega) + \sin(2\theta - \omega)]$$

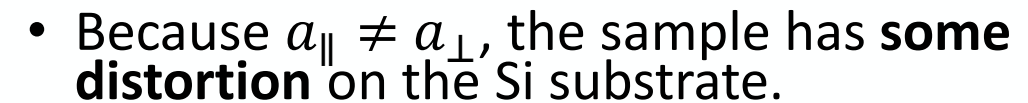
• Lattice constants:

•
$$a_{\parallel} = \frac{2\sqrt{2}}{s_{\chi}}$$
, $a_{\perp} = \frac{4}{s_{z}}$

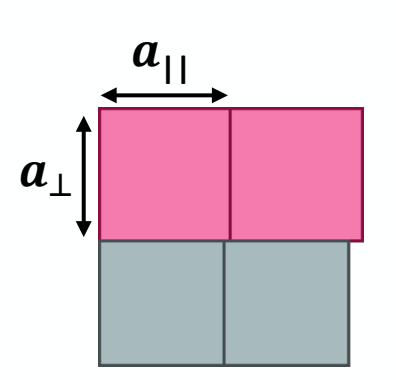


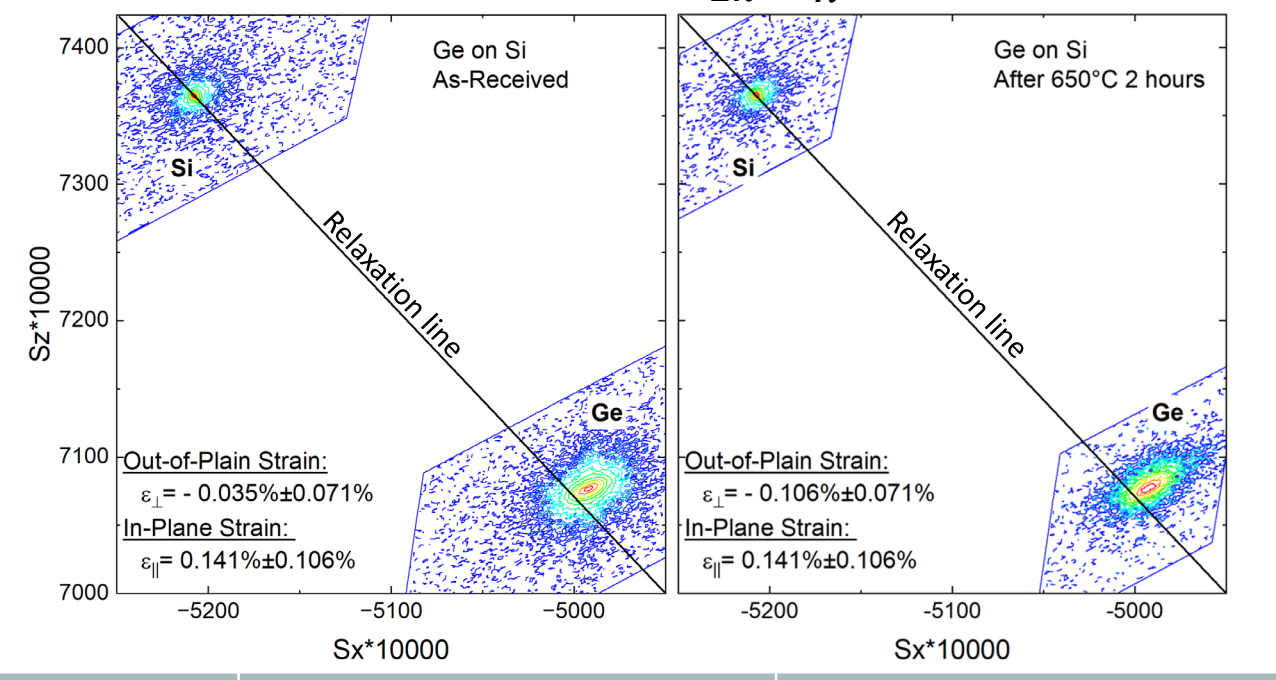
•
$$\varepsilon_{\parallel,\perp} = \frac{a_{\parallel,\perp} - a_{0,Ge}}{a_{0,Ge}}$$

• Bulk Ge $a_0 = 5.657$



- Tensile strain in parallel plane and compressive strain in perpendicular plane.
- Rapid thermal oxidation produces little to no increase in strain for Ge on Si.





	In-Plane		Out-of-Plane	
	a_{\parallel} (Å)	$arepsilon_{\parallel}$ (%)	a_{\perp} (Å)	$arepsilon_{\perp}$ (%)
As-Received:	5.665(0.006)	0.141(0.106)	5.655(0.004)	-0.0354(0.071)
650°C 2 hrs:	5.665(0.006)	0.141(0.106)	5.651(0.004)	-0.106(0.071)



Ge on Si: Oxidation Kinetics

• Deal-Grove Model: $t_{ox}^2 + At_{ox} = B(t + \tau)$;

• Oxide Thickness: t_{ox}

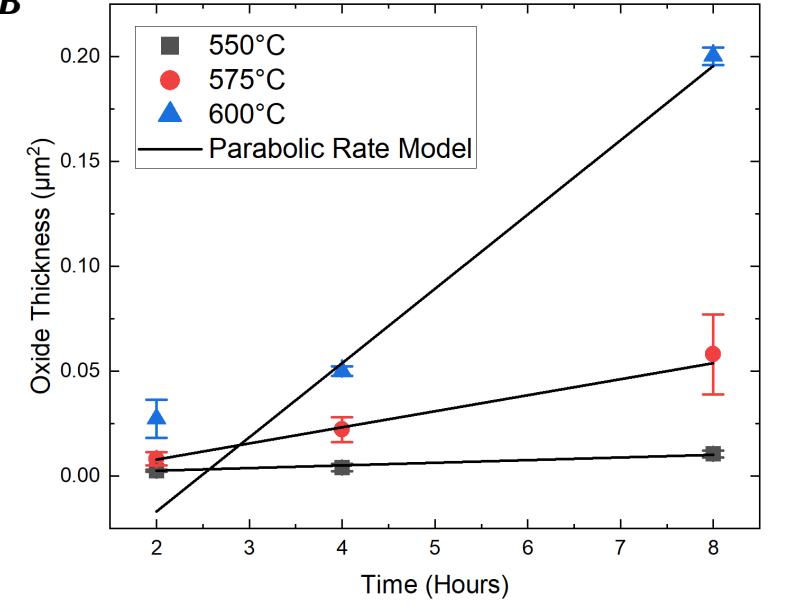
• Oxidation Time: t

• Oxidation Time Shift: $au = \frac{t_0^2 + At_0}{R}$

• For Thick Oxides: $(At_{ox} = 0)$

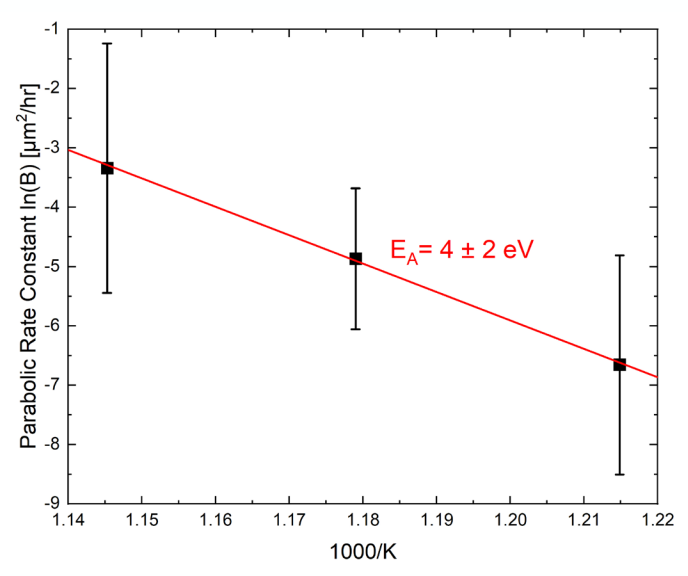
•
$$t_{ox}^2 \approx B(t+\tau)$$

Temp:	$B \left[\mu \text{m}^2 / \text{hr} \right]$	τ [hr]
550°C	0.0013(0.0024)	-0.02(5.24)
575°C	0.0077(0.0091)	-0.96(2.35)
600°C	0.0354(0.0744)	-2.48(6.01)



Parabolic Rate Constant: **B**

Linear Rate Constant: B/A

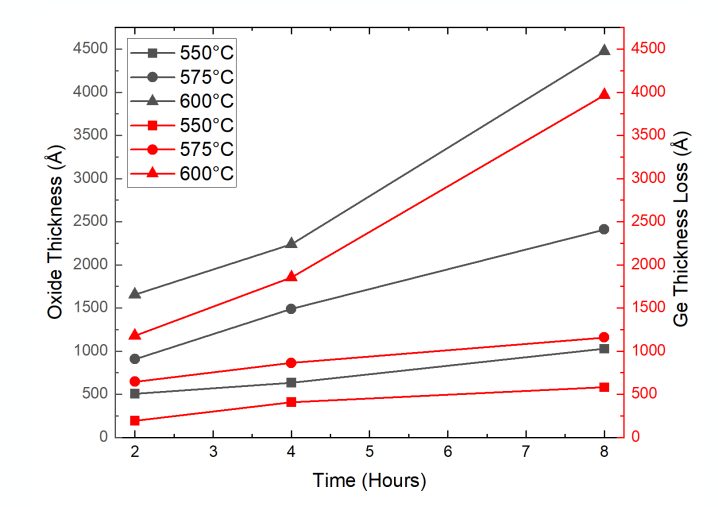


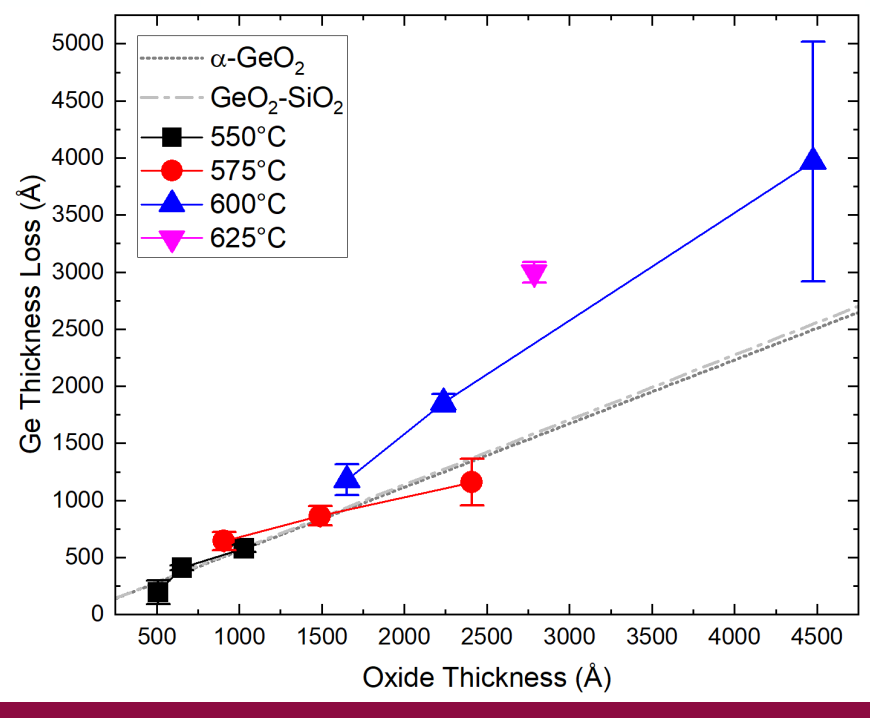
- Diffusion Coefficient:
 - $D \propto B = B_0 \exp[-E_a/kT]$
- Oxygen Diffusion in Ge on Si
 - Measured: $E_a = 4 \pm 2 eV$
- Oxygen Diffusion in pure Ge
 - Reported: $E_a = 2.02 \ eV$



Ge on Si: Oxidation Kinetics

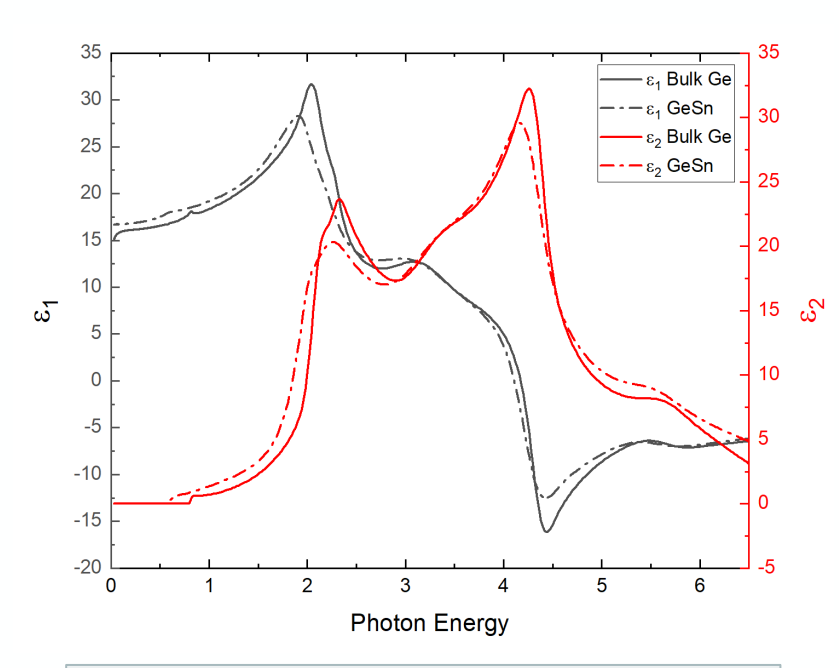
- During oxidation, oxygen reacts with Ge to form GeO₂
- Ge consumption: %Ge Consumption = $\frac{M_{Ge}/\rho_{Ge}}{M_{Oxide}/\rho_{Oxide}}$
- Bulk α -GeO₂: %Ge Con. = 0.56
 - $M = 104.\overline{5}9$ $\rho = 4.276$
- SiO₂-Substituted GeO₂: % Ge Con. = 0.57
 - M = 96.83 $\rho = 4.035$
- At higher temperatures:
 - Rate increased due to denser oxide of pure GeO₂
 - Rate increased due to more SiO₂-substitution
 - Rate of **Ge thickness loss increases** due to GeO₂ sublimating at higher temperatures



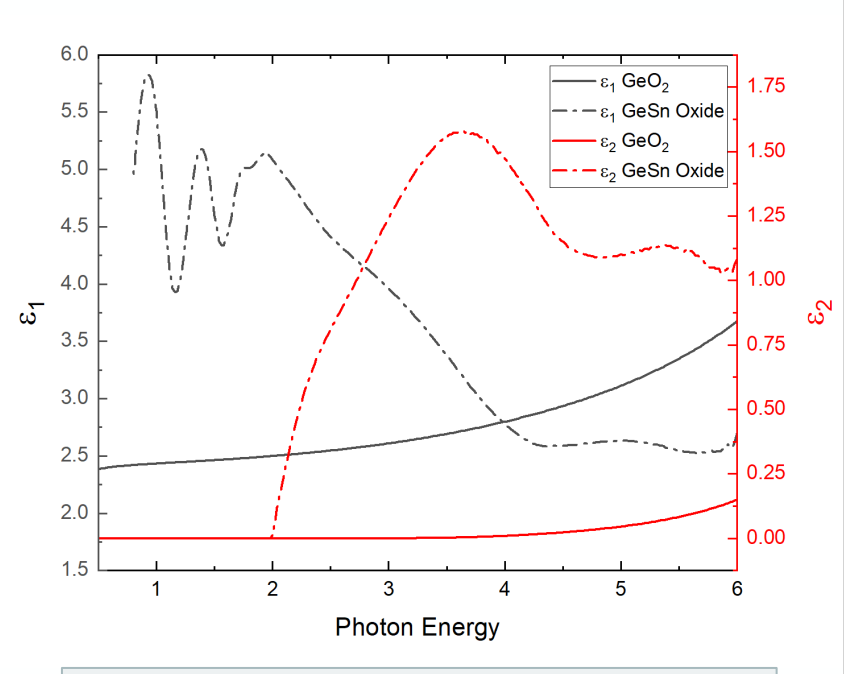




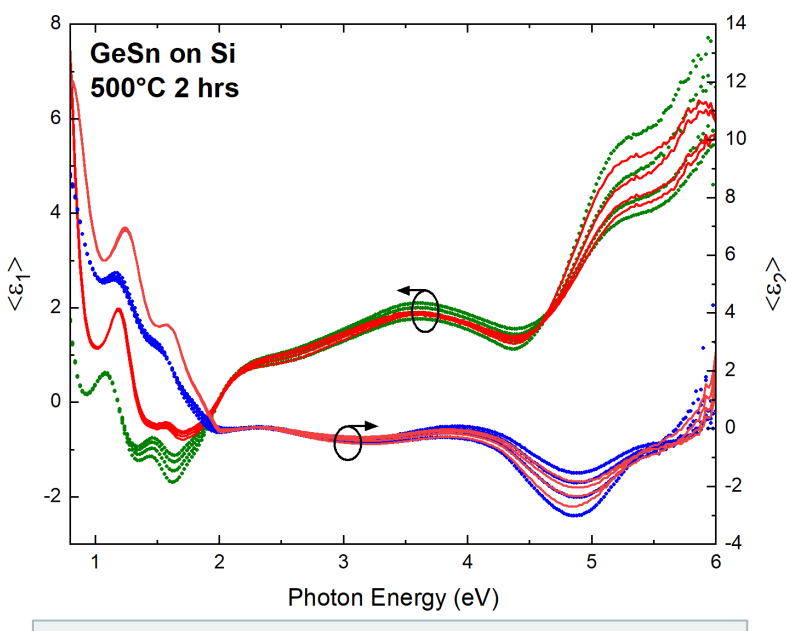
GeSn on Si: Optical Constants



Critical points of Ge's optical constants were modified for GeSn at 6.9% Sn.



Point-by-point fit for the oxide's optical constants to improve the model.



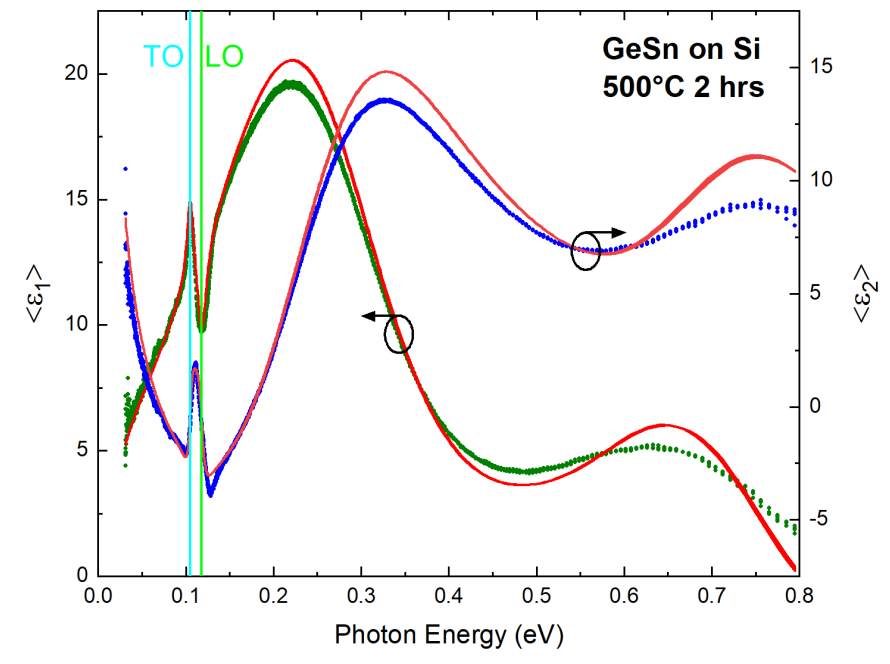
After anneal pseudodielectric function with non-uniformity within the GeSn and GeSn oxide layers.

Only reliable data that can be gathered is that the thickness of the oxide is about 600 Å.



GeSn on Si: IR Ellipsometry

- Because of the unreliable results of UVVASE, the after anneal thicknesses were determined with IRVASE.
- Model consisted of Drude model for the Si and GeSn layers. The oxide was modeled with a general oscillator layer.
- The **TO** and **LO** phonon frequencies were found to be **0.11 eV and 0.12 eV**, consistent with anisotropic trigonal GeO₂ (0.105-0.124 eV).



Pseudodielectric of GeSn on Si annealed at 500°C for 2 hours with labeled TO and LO phonon frequencies.

TO: Peak of ε_2

LO: Peak of Loss Function, $\operatorname{Im}\left(-\frac{1}{\varepsilon}\right) = \frac{\varepsilon_2}{\varepsilon_1^2 + \varepsilon_2^2}$

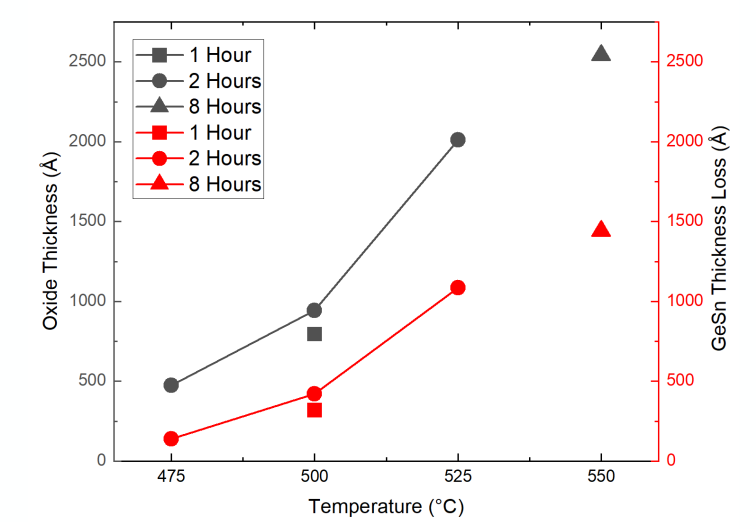


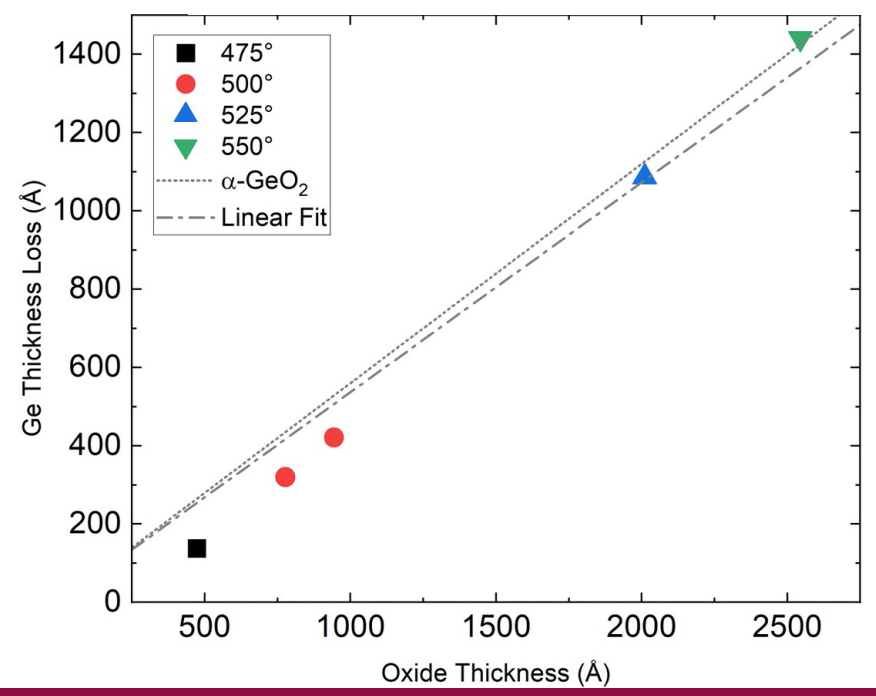
GeSn on Si: Oxidation Kinetics

- Oxide growth and loss of GeSn epilayer is similar that of the Ge epilayer on Si
- GeSn consumption rate was estimated with a linear fit through the origin where $\%GeSn\ Con. = 0.54$
 - Bulk α -GeO₂: %*Ge Con.* = **0.56**

BE BOLD. Shape the Future.[®]

• The small incorporation of Sn in the Ge slightly decreased the consumption of the epilayer

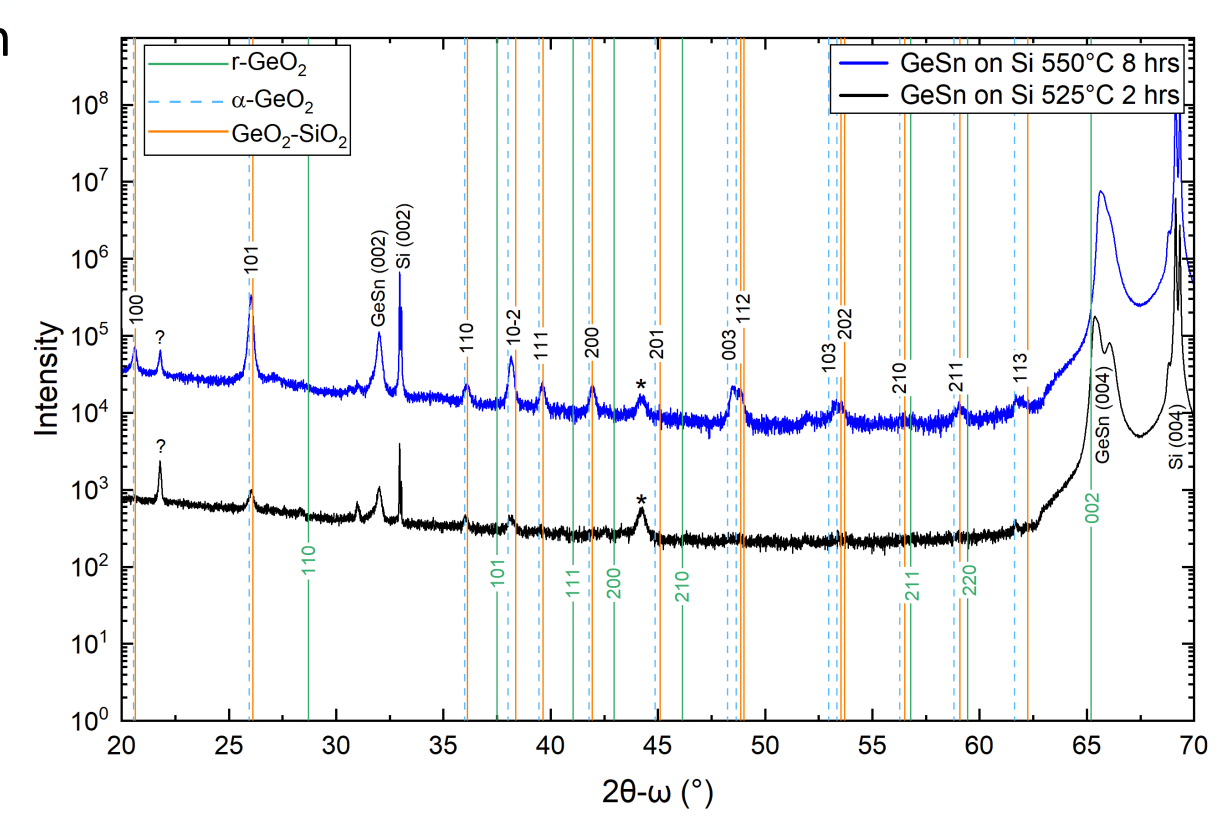






GeSn on Si: After Anneal Powder XRD

- After annealing new peaks, like Ge on Si, were seen on the spectra
- β -Sn powder 99.5% were compared to spectra, confirming none is present
- (004) **peak separates**, corresponding to Ge (004) and GeSn (004), caused by **Sn migration** in the epilayer.
- Higher temperature anneals show similar patterns to the oxide formed on Ge on Si
- Unknown peak at $2\theta=21^\circ$; if Si is present in epilayer, may correspond to cristobalite- β or an α -quartz ${\bf SiO_2}$.





GeSn on Si: High Resolution XRD

$$s_x = \frac{q_x}{2\pi} = \frac{1}{\lambda} [\cos(\omega) - \cos(2\theta - \omega)]$$
$$s_z = \frac{q_z}{2\pi} = \frac{1}{\lambda} [\sin(\omega) + \sin(2\theta - \omega)]$$

In-Plane and Out-of-Plane Lattice Constants:

•
$$a_{\parallel,\perp GeSn} = \frac{q_{\parallel,\perp Si} - q_{\parallel,\perp GeSn}}{q_{\parallel,\perp GeSn}} a_{Si} + a_{Si}$$

Relaxed Lattice Constant:

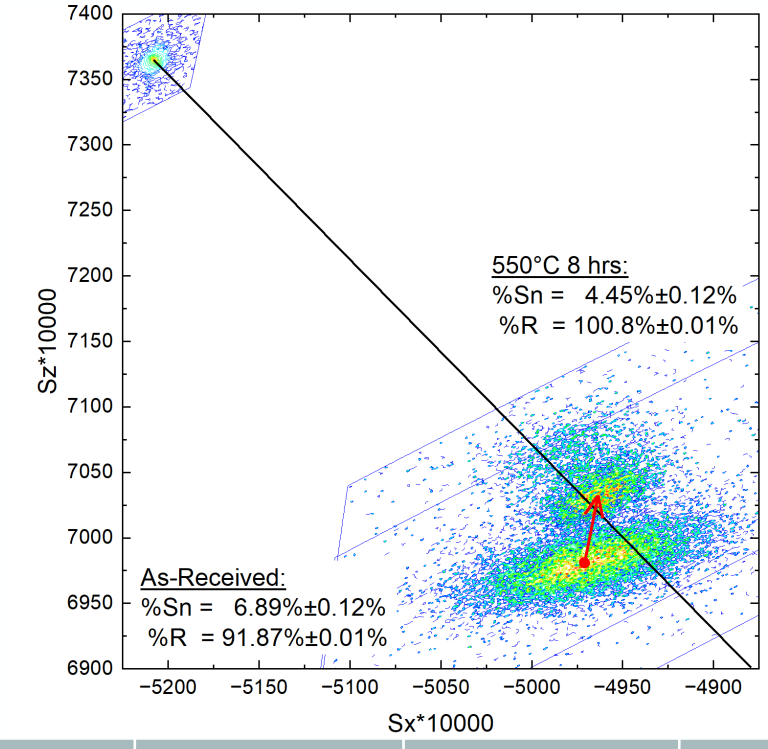
•
$$a_0 = a_\perp + \frac{2\nu_{GeSn}(a_{\parallel GeSn} - a_{\perp GeSn})}{1 + \nu_{GeSn}}$$

• Poisson's ratio:
$$v_{GeSn} = (1 - x)v_{Ge} + xv_{Sn}$$

Relaxation and Sn content:

•
$$\%R = \frac{a_{\parallel GeSn} - a_{Si}}{a_{0GeSn} - a_{Si}}, \quad \%Sn = \frac{a_{0GeSn} - a_{Ge}}{a_{0Sn} - a_{Ge}}$$

• Epilayer becomes more relaxed after anneal and Sn content is reduced.



	In-Plane	Out-of-Plane	Relaxed
	a_{\parallel} (Å)	a_{\perp} (Å)	a_0 (Å)
As-Received:	5.692(0.001)	5.731(0.001)	5.715(0.001)
650°C 2 hrs:	5.697(0.001)	5.693(0.001)	5.695(0.001)



Conclusion

- Ge on Si oxidation followed the parabolic rate model from the Deal-Grove model, leading to an Activation Energy of 4±2 eV.
- Both GeSn and Ge had phonon frequencies that were consistent with known values for trigonal GeO₂
- Non-uniformity of the surface layers caused complicated models.
- Powder diffraction confirmed the formation of α -GeO₂
- HRXRD determined that after annealing:
 - Ge on Si: little to no change in the strain of the epilayer
 - **GeSn on Si:** Epilayer relaxed and Sn loss

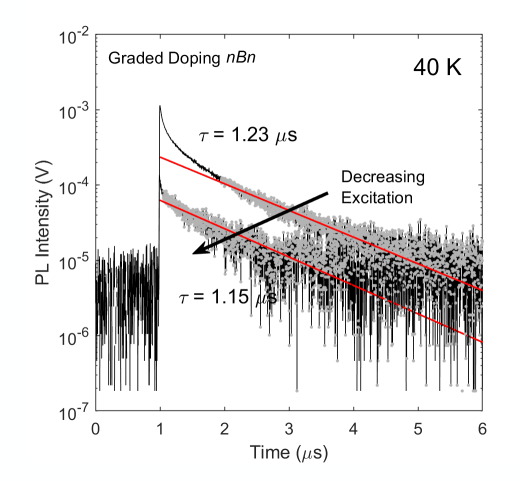


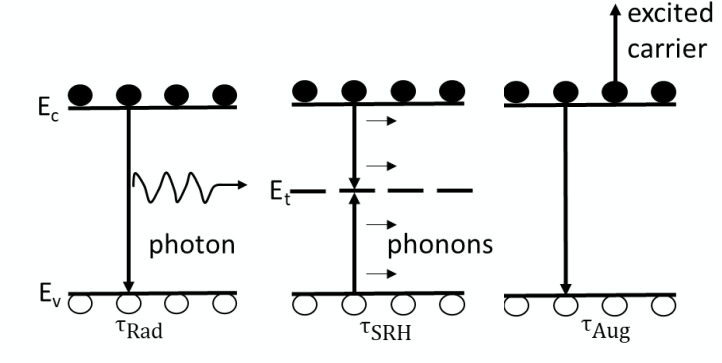
Temperature-Dependent Recombination Rate Analysis of Minority Carrier Lifetime in MidWave Infrared AntimonideBased Devices



Introduction

- A critical parameter is the Minority Carrier Lifetime (MCL) measured by Time-Resolved Photoluminescence.
 - time that a material stays in the excited state by **recording the time the material photoluminesces** before returning to the ground state.
- Model can be used to determine dominant recombination mechanisms
 - Radiative, Shockley-Read-Hall, Auger
- The MCL is affected by different parameters such as **strain engineering and localization.**
- Localization causes a **significant increase in the MCL** at low temperatures that does not predict material quality.





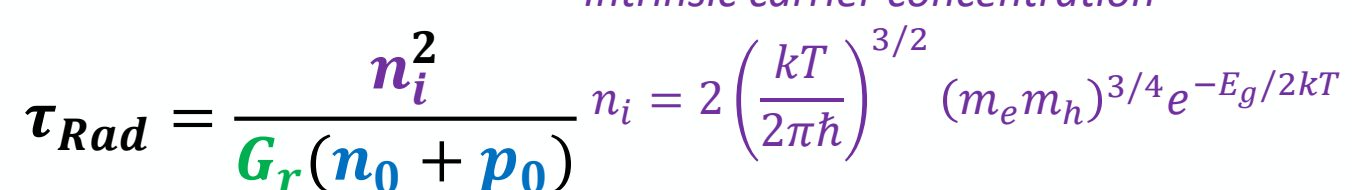


Recombination Mechanisms: Radiative

- Electron-hole pairs recombine, emitting a photon near the bandgap.
- More efficient in direct bandgap materials, then indirect.
- For intrinsic semiconductors, $n_i^2 = n_0 p_0$

BE BOLD. Shape the Future.®

• For n-type materials, Doping Density $N_D = n_0 - p_0$

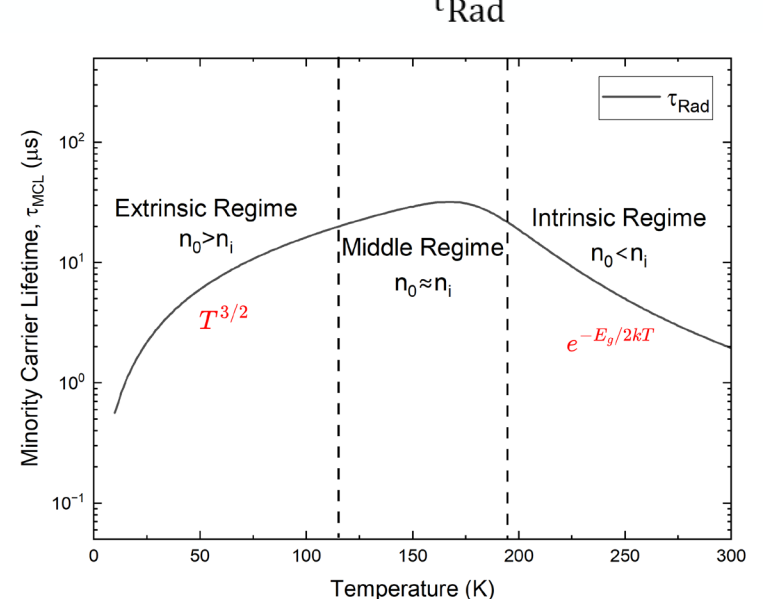


Radiative Generation Rate (Integrated thermal emissions spectrum; influenced by the temperature dependence of the bandgap, photon density, absorption coefficient, and *intrinsic carrier concentration)*

Intrinsic carrier concentration

$$n_i = 2 \left(\frac{kT}{2\pi\hbar}\right)^{3/2} (m_e m_h)^{3/4} e^{-E_g/2kT}$$

Electron and hole concentrations





I. Pelant et al., Channels of radiative recombination in semiconductors (2012).

C. Kittel, Introduction to Solid State Physics (John Wiley & Sons, New York, 1995).

R. Carrasco et al., J. Appl. Phys. **129**, 184501 (2021).

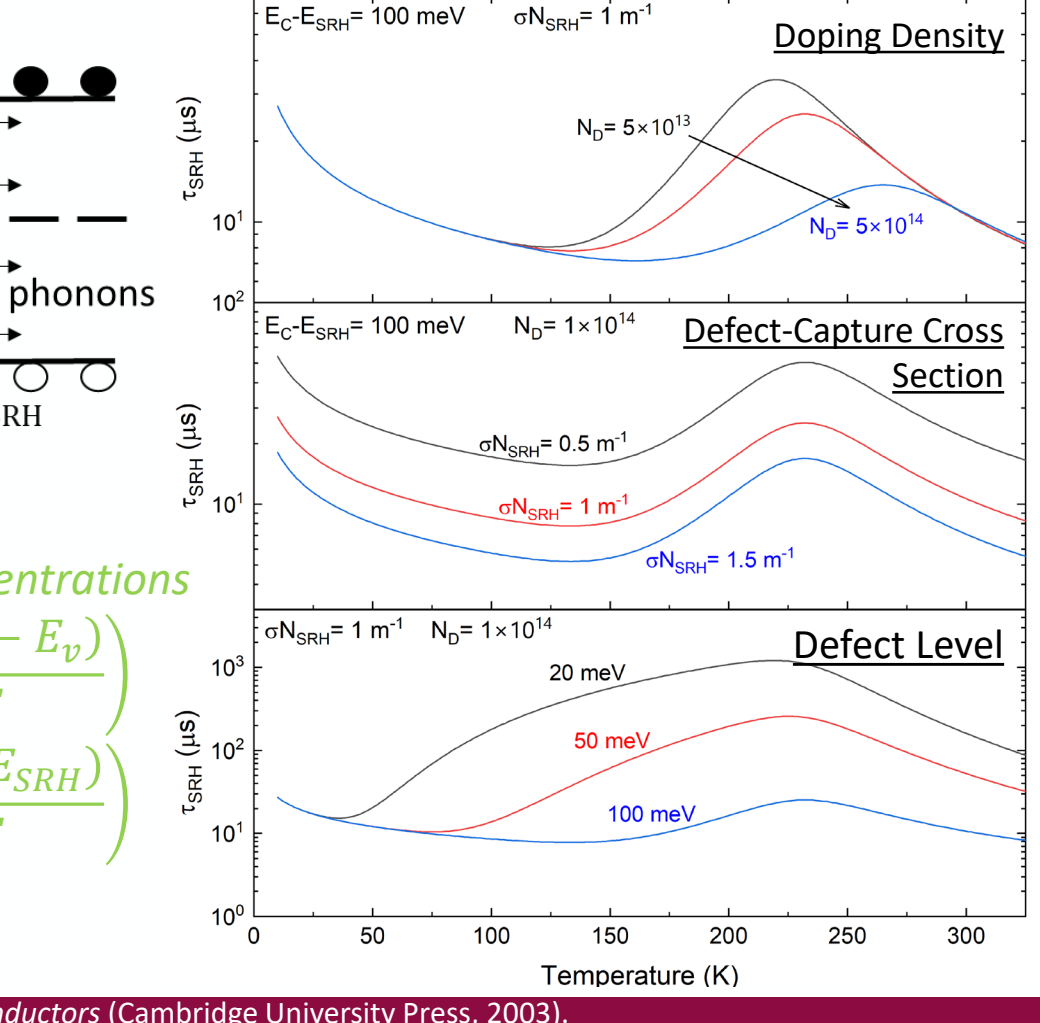
Recombination Mechanisms: SRH

- Photogenerated carriers recombine at trap states in the bandgap, which are caused by lattice defects and impurities.
- Non-radiative recombination

concentrations



$$p_1 = n_i \exp\left(\frac{-(E_{SRH} - E_v)}{k_B T}\right)$$
 $n_1 = n_i \exp\left(\frac{-(E_c - E_{SRH})}{k_B T}\right)$
 $n_1 = n_i \exp\left(\frac{-(E_c - E_{SRH})}{k_B T}\right)$



 E_C - E_{SRH} = 100 meV



 τ_{SRH}

superlattices (2012).

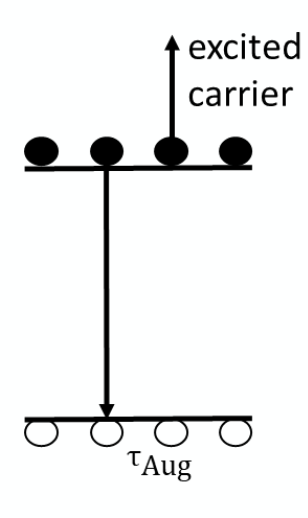
I. Pelant et al., Non-radiative recombination (2012).

R. Carrasco et al., J. Appl. Phys. **129**, 184501 (2021).

P. Webster et al., J. Appl. Phys. 133, 125704 (2023).

Recombination Mechanism: Auger

- Excess energy is transferred to a third charge carrier sending that carrier to higher energy state.
- Non-radiative recombination, that dissipates as heat.
- Auger-1 coefficient describes electron-electron collisions that occur in the conduction band
- For n-type doping, $m_h > m_e$ making other **Auger processes negligible**.



Intrinsic carrier concentration

$$au_{Auger} = rac{2n_i^2}{n_0^2 + n_0 p_0} imes au_{A1}$$

Electron and hole concentrations

$$\tau_{Auger} = \frac{2n_i^2}{n_0^2 + n_0 p_0} \times \tau_{A1}$$

$$\tau_{A1} = \frac{3.8 \times 10^{-18} \epsilon_{\infty}^2 (1 - \gamma)^{\frac{1}{2}} (1 + 2\gamma)}{(m_e/m_0)|F_1 F_2|^2} \times \left(\frac{E_g}{kT}\right)^{3/2} \exp\left(\frac{1 + 2\gamma}{1 + \gamma} \frac{E_g}{kT}\right)$$

$$\tau_{A1} = \frac{3.8 \times 10^{-18} \epsilon_{\infty}^2 (1 - \gamma)^{\frac{1}{2}} (1 + 2\gamma)}{(m_e/m_0)|F_1 F_2|^2} \times \left(\frac{E_g}{kT}\right)^{3/2} \exp\left(\frac{1 + 2\gamma}{1 + \gamma} \frac{E_g}{kT}\right)$$

$$\tau_{A1} = \frac{m_e}{m_b}$$



superlattices (2012).

I. Pelant et al., Non-radiative recombination (2012).

A. Beattie et al., Proc. R. Soc. Lond. A **249**, 16 (1959).

R. Carrasco et al., J. Appl. Phys. **129**, 184501 (2021).

Previous Observations: Strain Engineering

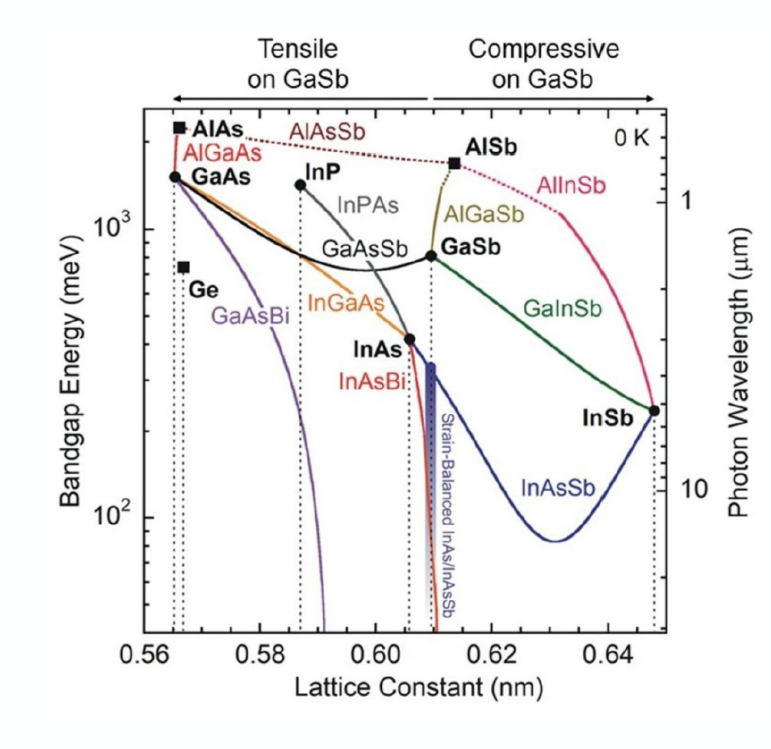
 Strain balanced InAs/InAsSb superlattices are used in midwave infrared (MWIR) sensing due to their tunable cutoff wavelength.

• Problem:

• Strain-balance conditions are required to grow thick InAs/InAsSb superlattice active regions. InAs layers must be thicker resulting in wide potential wells for electrons and holes are confined in the narrow wells of the InAsSb layers.

• *Theory*:

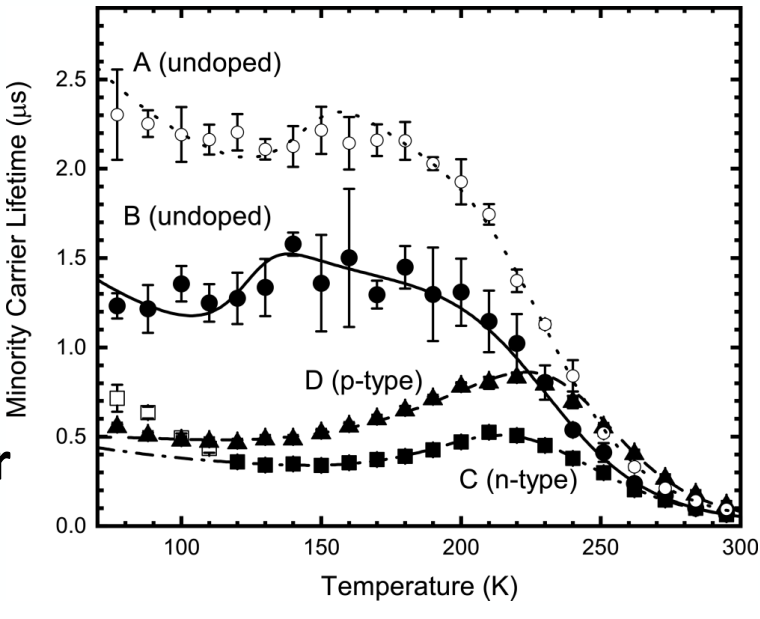
• By incorporating Ga to create InGaAs, the lattice constant can be adjusted, **reducing the compressive tensile mismatch** to create more balanced layer thickness.





Previous Observations: Strain Engineering

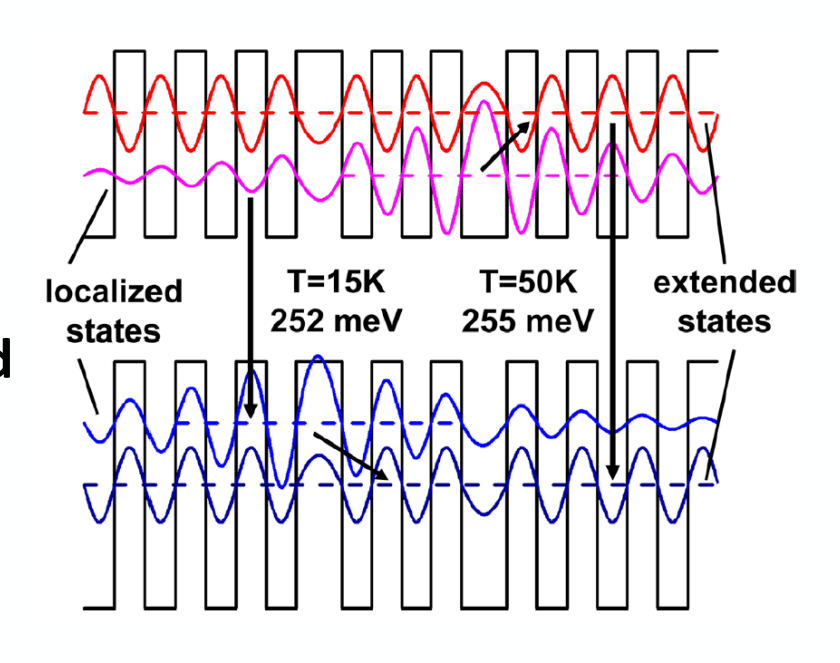
- Samples to evaluate the incorporation of Ga:
 - A: Undoped InAs/InAsSb SL- Reference
 - B: Undoped InGaAs/InAsSb SL 20% Ga
 - C: p-type npBp InGaAs/InAsSb SL npBp structure
 - D: n-type *nBn* InGaAs/InAsSb SL *–nBn structure*
- The Ga incorporation:
 - slightly reduced the minority carrier lifetime but increases carrier diffusion length, $L_D=(D\tau_{mc})^{1/2}$, improving carrier transport
 - Doped samples are **SRH limited** at 0.5 μ s at <120 K which is **favorable for MWIR applications**. 0.5 μ s is considered long especially with the **increased mobility that Ga incorporation** enables





Previous Observations: Localization Effects

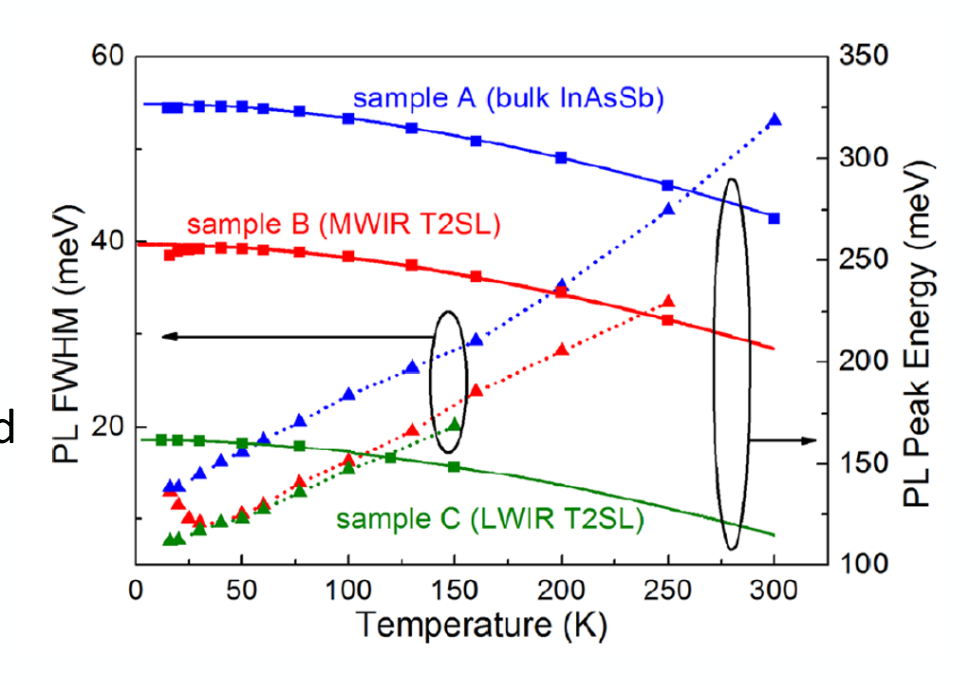
- In a study by Lin et al., InAs/InAsSb SL had a minority carrier lifetime of 12.8 μs at 15 K using time-resolved photoluminescence
- Not caused by high material quality, but rather *Carrier Localization*:
 - Localization occurs when electrons and holes become trapped in random potential wells caused by structural disorder.
 - Thickness fluctuations causes potential minima that act as localization centers
 - Trapped carriers occupy separated localized states, slowing recombination, leading to belief of high material quality.





Previous Observations: Localization Effects

- Samples to investigate the cause of the long minority lifetime:
 - A: Bulk InAsSb Reference
 - B: MWIR InAs/InAsSb SL -Short Period (12.8 μs lifetime at 15 K)
 - C: LWIR InAs/InAsSb SL Long Period
- Steady-state photoluminescence from 15 K 300 K revealed the localization.
 - FWHM broadened below 40 K Carriers reside in localized states, exhibiting different Fermi levels due to various localization centers.
 - Sample B blue shifted by 3 meV from 15 K to 50 K carriers delocalize as temperature increases. After, carriers occupy extended states.
- Localization was specific to short-period MWIR SL.
- This reveals that localization needs to be identified and taken into account when studying InAs/InAsSb superlattices.

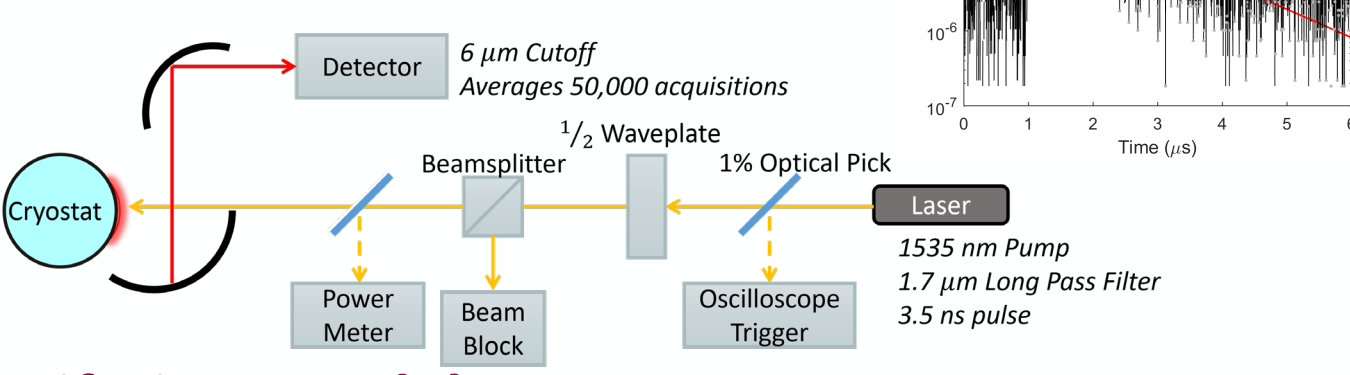


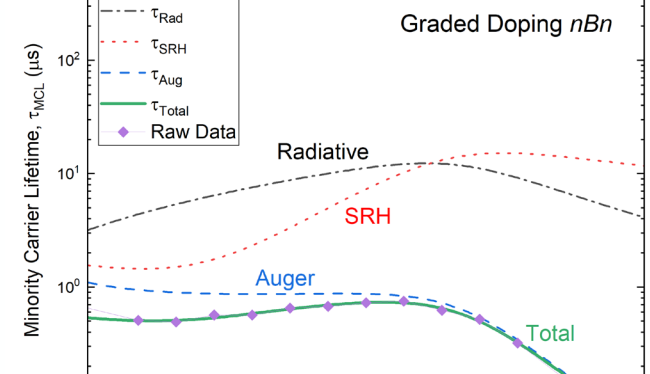


Time-Resolved Photoluminescence

- Measurement of the amount of time that a material stays in the excited state by recording the time the material photoluminesces before returning to the ground state.
- Liquid helium (~5 K to 77 K); Liquid Nitrogen (77 K-300 K).

250





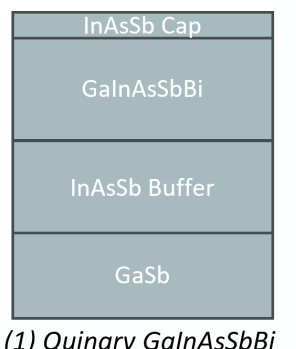
Temperature (K)

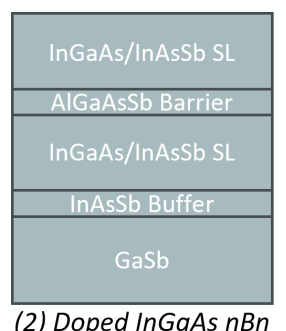
Recombination Lifetime Model

Minority Carrier Lifetime:

•
$$\frac{1}{\tau_{\text{MCL}}} = \frac{1}{\phi \tau_{\text{rad}}} + \frac{1}{\tau_{\text{SRH}}} + \frac{1}{\tau_{\text{Auger}}}$$

- ϕ -photon recycling factor
- Gives insight into dominant material's quality, recombination mechanisms, and defect density.



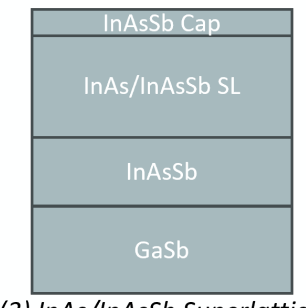


Graded Doping nBn

au = 1.23 μ s

 10^{-3}

PL Intensity (V)



40 K

Decreasing

(1) Quinary GalnAsSbBi

(3) InAs/InAsSb Superlattice



100

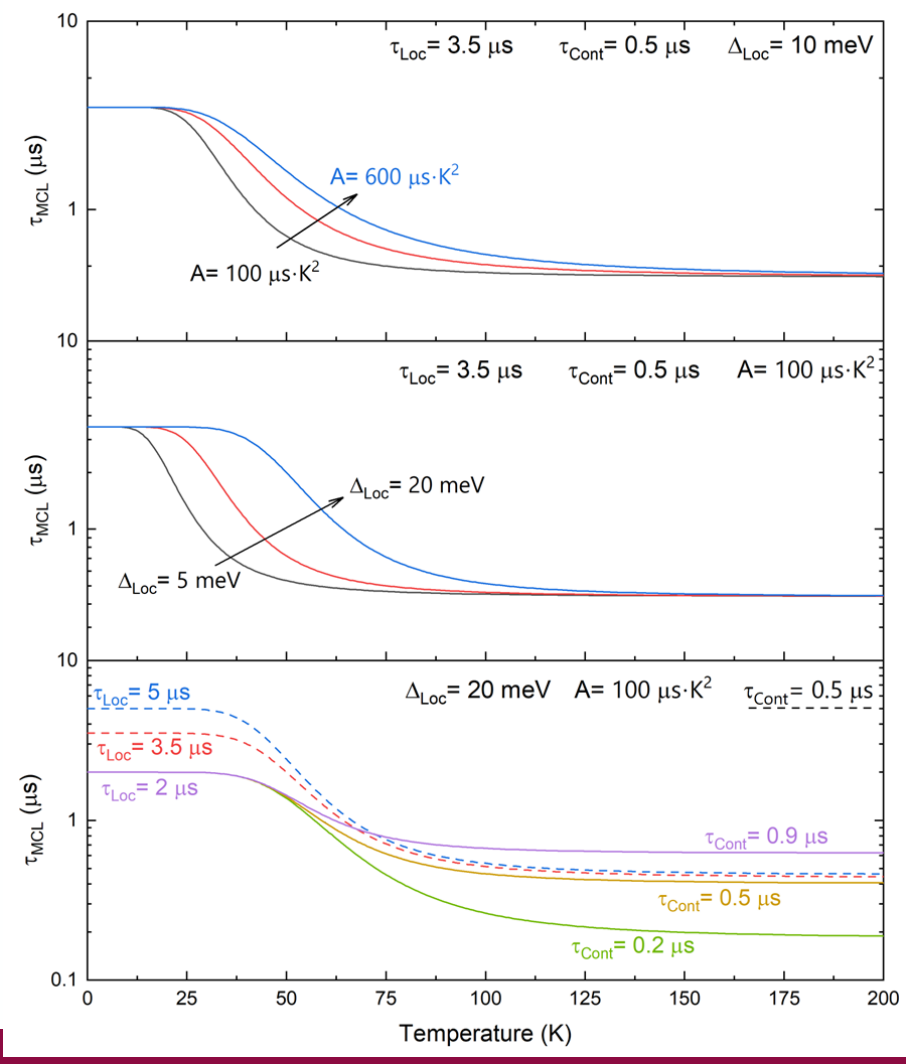
Trap-Delayed Recombination Model

• At low temperatures (<100 K), MCL increases significantly **due to localization**.

• Modeled by:
$$\frac{1}{\tau_{MCL}} = \frac{1}{\tau_{Loc}} + \frac{1}{\tau_{Emis} + \tau_{Cont}};$$

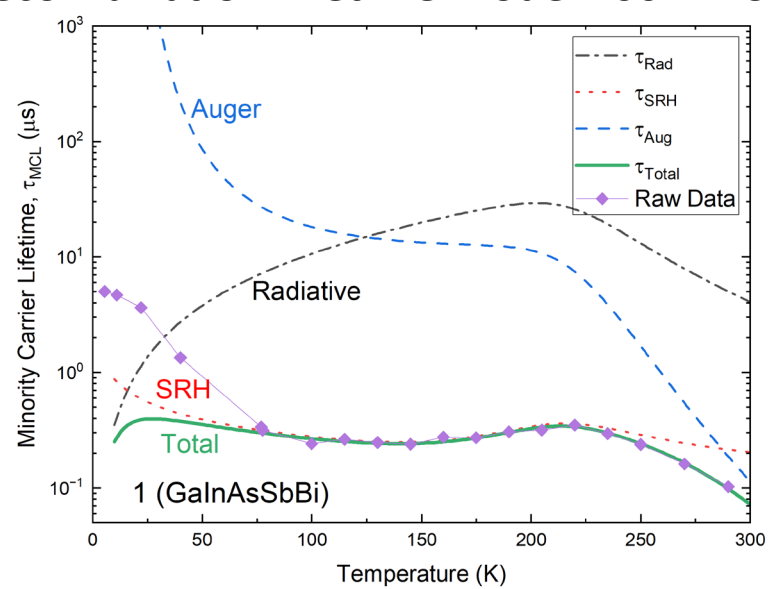
•
$$\tau_{Emis} = \frac{A}{T^2} \exp\left(\frac{\Delta_{Loc}}{kT}\right)$$

- τ_{Loc} Initial lifetime due to localization.
- Δ_{Loc} Temperature carriers escape to extended states.
- A- Rate of carriers that are released.
- τ_{Cont} Lifetime at extended states.



(1) GaInAsSbBi

Recombination Lifetime Model 100 K – 300 K

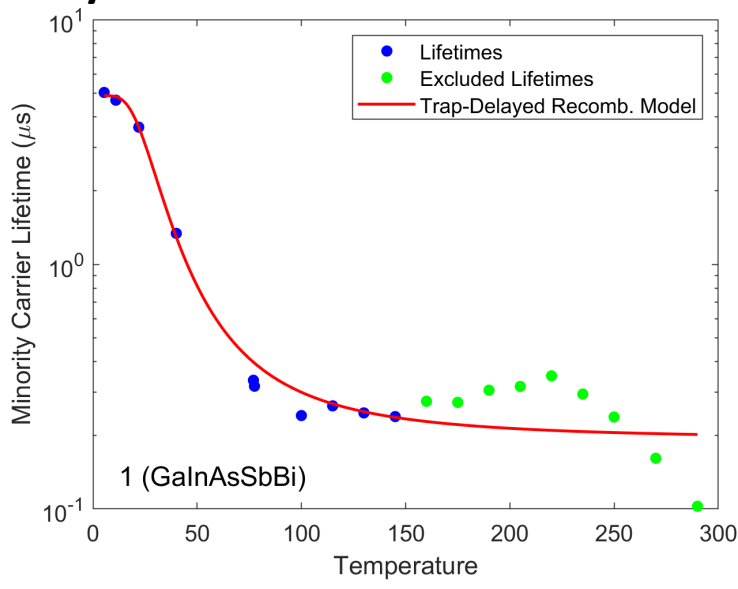


Doping Density (x10 15 cm $^{-3}$) N_D	0.71
Defect Level (meV) $E_{\it C}-E_{\it SRH}$	79.6
Defect Density (m ⁻¹) $\sigma N_{ m SRH}$	31.0
Bloch Overlap Integral $ F_1F_2 $	0.50

From 100 K – 225 K, SRH dominates.

Then drops due to Auger recombination due to large Bloch overlap integral.

Trap-Delayed Recombination Model ~5 K – 150 K



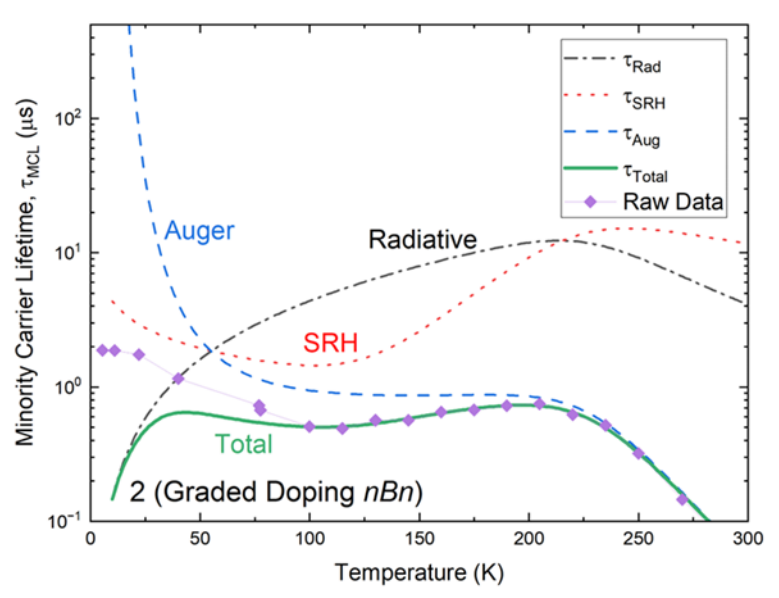
Energy Separation (meV) $\Delta_{ ext{Loc}}$	4.20
Loc. State Lifetime (μ s) $ au_{ m Loc}$	4.89
Amplitude (μ s · K^2) A	735
Cont. Lifetime (μ s) $ au_{ m Cont}$	0.2

Longest τ_{Loc} suggesting carriers may remain trapped for longer intervals.



(2) Graded Doping *nBn*

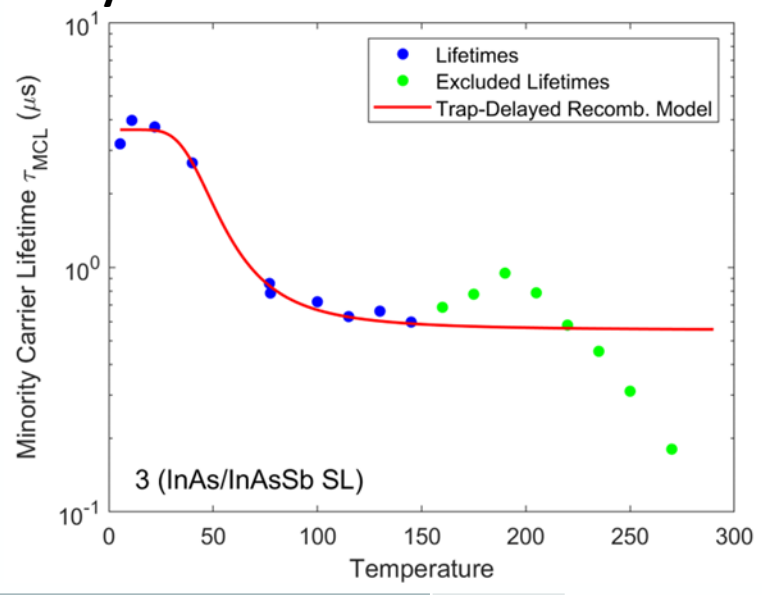
Recombination Lifetime Model 100 K – 300 K



Doping Density (x10 15 cm $^{-3}$) N_D	6.29
Defect Level (meV) $E_{\it C}-E_{\it SRH}$	1.65
Defect Density (m $^{ ext{-1}}$) $\sigma N_{ m SRH}$	6.21
Bloch Overlan Integral $ F_1F_2 $	0.15

SRH and Auger are at the same magnitude until about 150 K, neither are dominating in this region.

Trap-Delayed Recombination Model ~5 K – 150 K



Energy Separation (meV) $\Delta_{ ext{Loc}}$	2.80
Loc. State Lifetime (μ s) $ au_{ m Loc}$	1.89
Amplitude (μ s \cdot K^2) A	1970
Cont. Lifetime (μ s) $ au_{ ext{Cont}}$	0.5

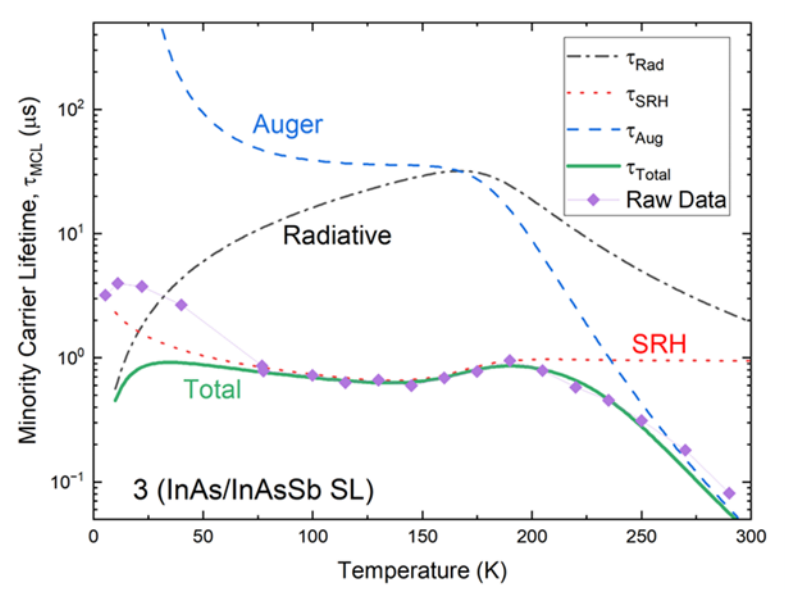
Lowest Δ_{Loc} and shortest τ_{Loc} but largest A.

Carriers may escape more easily.



(3) InAs/InAsSb SL

Recombination Lifetime Model 100 K – 300 K

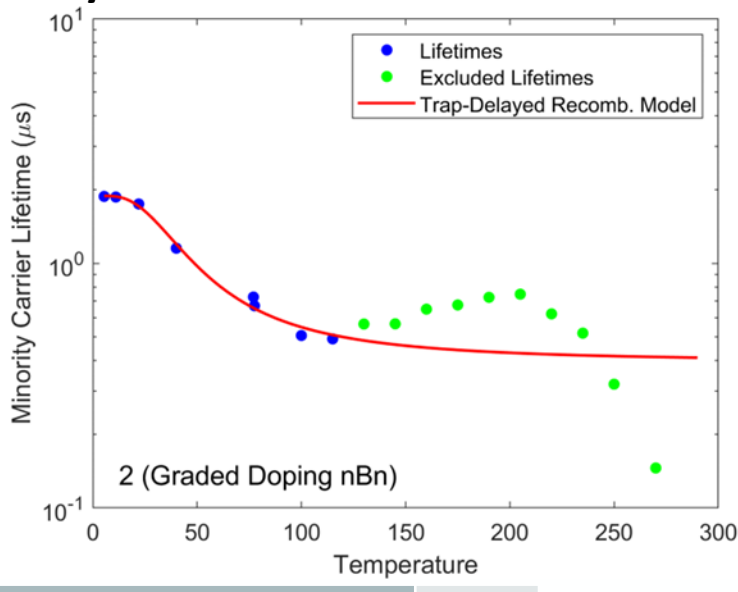


Doping Density (x10 15 cm $^{-3}$) N_D	0.79
Defect Level (meV) $E_{\it C}-E_{\it SRH}$	108
Defect Density (m $^{ ext{-1}}$) $\sigma N_{ m SRH}$	11.7
Bloch Overlap Integral $ F_1F_2 $	0.19

From 100 K – 200 K, SRH dominates.

From 200 K – 300 K, Auger dominates.

Trap-Delayed Recombination Model ~5 K – 125 K



Energy Separation (meV) $\Delta_{ ext{Loc}}$	12.5
Loc. State Lifetime (μ s) $ au_{ m Loc}$	3.65
Amplitude (μ s · K^2) A	396
Cont. Lifetime (μ s) $ au_{ m Cont}$	0.65

Largest Δ_{Loc} indicate stronger confinement of carriers from structural disorder in SL.



Conclusion

- Demonstrated the temperature-dependent analysis of the minority carrier lifetime using **time-resolved photoluminescence**.
- Dominant recombination mechanisms and the effects of localization were determined by the *Recombination Lifetime* and the *Trap-Delayed Recombination Model*.
- The minority carrier lifetime can be affected by different factors like strain engineering or depend on the device.

